Metallic Behavior and Periodical Valence Ordering in a MMX Chain Compound, $Pt_2(EtCS_2)_4I$

Minoru Mitsumi,*,† Tomoko Murase,† Hideyuki Kishida,† Tetsuya Yoshinari,† Yoshiki Ozawa,† Koshiro Toriumi,*,† Takuya Sonoyama,‡ Hiroshi Kitagawa,‡,§ and Tadaoki Mitani‡

Contribution from the Department of Material Science, Himeji Institute of Technology, 3-2-1 Kouto, Kamigori-cho, Hyogo 678-1297, Japan, and Japan Advanced Institute of Science & Technology, Tatsunokuchi, Ishikawa 923-1292, Japan

Received April 9, 2001

Abstract: A new one-dimensional (1-D) halogen-bridged mixed-valence diplatinum(II,III) compound, $Pt_2(EtCS_2)_4I$ (**3**), has been successfully synthesized from $[Pt_2(EtCS_2)_4]$ (**1**) and $[Pt_2(EtCS_2)_4I_2]$ (**2**). These three compounds have been examined using UV−visible−near-IR, IR, polarized Raman spectroscopy, X-ray photoelectron spectroscopy (XPS), and X-ray crystal structure analyses (except for **1**). Compound **3** was further characterized through electrical transport measurements, determination of the temperature dependence of lattice parameters, X-ray diffuse scattering, and SQUID magnetometry. **3** crystallizes in the monoclinic space group *C*2/*c* and exhibits a crystal structure consisting of neutral 1-D chains with a repeating −Pt−Pt−I− unit lying on the crystallographic 2-fold axis parallel to the *b* axis. The Pt−Pt distance at 293 K is 2.684 (1) Å in the dinuclear unit, while the Pt−I distances are essentially equal (2.982 (1) and 2.978 (1) Å). **3** shows relatively high electrical conductivity (5−30 S cm^{-1}) at room temperature and undergoes a metal−semiconductor transition at $T_{M-S} = 205$ K. The XPS spectrum in the metallic state reveals a Pt^{2+} and Pt^{3+} mixed-valence state on the time scale of XPS spectroscopy ($\sim 10^{-17}$ s). In accordance with the metal−semiconductor transition, anomalies are observed in the temperature dependence of the crystal structure, lattice parameters, X-ray diffuse scattering, and polarized Raman spectra near T_{M-S}. In variable-temperature crystal structure analyses, a sudden and drastic increase in the Pt−I distance near the transition temperature is observed. Furthermore, a steep increase in U_{22} of iodine atoms in the 1-D chain direction has been observed. The lattice parameters exhibit significant temperature dependence with drastic change in slope at about 205−240 K. This was especially evident in the unit cell parameter *b* (1-D chain direction) as it was found to lengthen rapidly with increasing temperature. X-ray diffraction photographs taken utilizing the fixed-film and fixed-crystal method for the metallic state revealed the presence of diffuse scattering with line shapes parallel to the a^* axis indexed as $(-, n + 0.5, l)$ (n; integer). Diffuse scattering with $k = n + 0.5$ is considered to originate from the 2-fold periodical ordering corresponding to $-Pt^{2+}-Pt^{2+}-I-Pt^{3+}-Pt^{3+}-I-$ or $-Pt^{2+}-Pt^{3+}-I-Pt^{3+}-Pt^{2+}-I-$ in an extremely short time scale. Diffuse lines corresponding to 2-D ordering progressively decrease in intensity below 252 K and are converted to the diffuse planes corresponding to 1-D ordering near T_{M-S}. Furthermore, diffuse planes condensed into superlattice reflections below T_{M-S}. Polarized Raman spectra show temperature dependence through a drastic low-energy shift of the Pt−I stretching mode and also through broadening of bands above T_{M-S}.

Introduction

For several decades there has been considerable interest in quasi-one-dimensional (1-D) halogen-bridged mixed-valence metal complexes, MX chain compounds,[1] because of their characteristic physical properties such as strong intervalence charge-transfer (IVCT) absorption,[2] luminescence with a large Stokes shift,[3] and resonance Raman scattering with high overtone progression originating from strong electron−lattice interactions.[4] MX compounds with M = Pt, Pd exhibit a large distortion in the position of halogen atoms from the midpoint between two metal atoms due to Peierls instability. Their ground-state structures are best described as a charge density wave (CDW) state. In the case of nickel compounds, bridging halogen atoms are located at the midpoint between two Ni atoms due to strong electron correlation. These compounds are Mott−

† Himeji Institute of Technology.

‡ Japan Advanced Institute of Science & Technology.

§ Present address: Department of Chemistry, University of Tsukuba, Tsukuba 305-8571, Japan.

(1) (a) *Low-dimensional Cooperative Phenomena*; Keller, H. J., Ed.; NATO ASI Series, Series B; Plenum Press: New York, 1975; Vol. 7. (b) Day. P. In *Chemistry and Physics of One-Dimensional Metals*; Keller, H. J., Ed.; NATO ASI Series, Series B; Plenum Press: New York, 1977; Vol. 25, pp 197−223. (c) Soos, Z. G.; Keller, H. J. In *Chemistry and Physics of One-Dimensional Metals*; Keller, H. J., Ed.; NATO ASI Series, Series B.; Plenum Press: New York, 1977; Vol. 25, pp 391−412. (d) Day, P. In *The Physics and Chemistry of Low Dimensional Solids*; Alcácer, L. Ed.; NATO ASI Series, Series C.; D. Reidel Publishing: Dordrecht, The Netherlands, 1980; Vol. 56, pp 305−320. (e) Keller, H. J. In *The Physics and Chemistry of Low Dimensional Solids*; Alcácer, L. Ed.; NATO ASI Series, Series C.; D. Reidel Publishing: Dordrecht, The Netherlands, 1980; Vol. 56, pp 321−331. (f) Keller, H. J. In *Extended Linear Chain Compounds*; Miller, J. S. Ed,; Plenum Press: New York, 1983; Vol. 1, Chapter 8. (g) Clark, R. J. H. *Adv. Infrared Raman Spectrosc.* **1984**, *11*, 95−132. (h) Clark, R. J. H. *Chem. Soc. Rev.* **1990**, *19*, 107−131.

(2) (a) Yamada, S.; Tsuchida, R. *Bull. Chem. Soc. Jpn.* **1956**, *29*, 894−898. (b) Wada, Y.; Mitani, T.; Yamashita, M.; Koda, T. *J. Phys. Soc. Jpn.* **1985**, *54*, 3143−3153. (c) Okamoto, H.; Toriumi, K.; Mitani, T.; Yamashita, M. *Phys. Rev. B* **1990**, *42*, 10381−10387.

(3) (a) Tanino, H.; Nakahara, J.; Kobayashi, K. *J. Phys. Soc. Jpn. Suppl.* **1980**, *49*, 695. (b) Tanaka, M.; Kurita, S.; Okada, Y.; Kojima, T.; Yamada, Y. *Chem. Phys.* **1985**, *96*, 343−348.

(4) (a) Clark, R. J. H.; Franks, M. L.; Trumble, W. R. *Chem. Phys. Lett.* **1976**, *41*, 287−292. (b) Clark, R. J. H.; Kurmoo, M. *Inorg. Chem.* **1980**, *19*, 3522−3527. (c) Tanino, H.; Kobayashi, K. *J. Phys. Soc. Jpn.* **1983**, 52, 1446−1456.

10.1021/ja010900v CCC: $20.00
Published on Web 10/18/2001

Hubbard semiconductors and their ground-state structures are described as a spin density wave (SDW) state.[2c,5] The nature of the ground state of MX chains is governed by competition between electron−lattice interactions and electron correlation. These MX compounds do not exhibit any dynamic physical properties due to strong stabilization through band gap formation; however, they may be excited by relatively high-energy radiation such as visible or ultraviolet light.

Recently, 1-D halogen-bridged mixed-valence dinuclear metal complexes, MMX chain compounds, have attracted significant attention. Previously, only two families of MMX chain compounds, namely, $A_4[Pt_2(pop)_4X]\cdot nH_2O$ ($pop = P_2O_5H_2^{2-}$; A = Li, K, Cs, NH_4; X = Cl, Br, I)[6] and $M_2(dta)_4I$ ($dta = CH_3CS_2^-$; M = Ni, Pt),[7−11] have been reported. These compounds exist in a mixed-valence state composed of M^{2+} (d^8) and M^{3+} (d^7) with a formal oxidation number of +2.5. Therefore, the MMX chain is a 1-D chain system based on a dinuclear unit containing a metal−metal bond with a formal bond order of $^1/_2$. The characteristic difference between these families lies in the charge of the chains. The former is composed of an anionic MMX chain necessitating countercations, while the latter is composed of an electrically neutral chain. Important features of MMX compounds are expected to arise from the increase in internal degrees of freedom resulting from the mixed-valence state of the dinuclear unit. MMX chains may adopt a variety of electronic structures represented by the following four extreme valence-ordering states.

(a) averaged valence state:

$$-M^{2.5+}-M^{2.5+}-X-M^{2.5+}-M^{2.5+}-X-$$

(b) charge-polarization state:

$$-M^{2+}-M^{3+}-X-M^{2+}-M^{3+}-X-$$

(c) charge density wave state:

$$-M^{2+}-M^{2+}-X-M^{3+}-M^{3+}-X-$$

(d) alternate charge-polarization state:

$$-M^{2+}-M^{3+}-X-M^{3+}-M^{2+}-X-$$

The valence state expressed as a $-M^{2+}-M^{3+}-$ represents an extreme case that is more accurately presented as $-M^{(2+\delta)+}-M^{(3-\delta)+}-$. The value of δ is dependent on the degree of orbital hybridization and lies between the limiting cases of 0 and 0.5. These valence-ordering states are classified on the basis of the periodicity of the 1-D chain. Thus, valence-ordering states in which periodicity of the 1-D chain is M−M−X−, (a) and (b), correspond to a metallic state with an effective half-filled conduction band mainly composed of M−M $d\sigma^*$−X p_z or to a Mott−Hubbard semiconducting state ($4k_F$-CDW), respectively. However, periodicity of the 1-D chain in valence-ordering states c and d are doubled and these electronic structures are regarded as Peierls ($2k_F$-CDW) and spin-Peierls ($2k_F$) states,[12] respectively. Valence-ordering states, with the exception of (a), are expected to exhibit lattice distortion due to valence alternations. The magnitude of the on-site Coulomb repulsion U in MMX compounds is relatively small in comparison to MX compounds due to the sharing of one unpaired electron through a metal−metal bond. This facilitates valence delocalization and enhances valence fluctuation in the mixed-valence state. In addition, significant one-dimensionality in the crystal structure is also a characteristic of MMX compounds. Intrachain interaction of the Pt−Pt or Pt−I coordination bond is much stronger than interchain Coulomb or van der Waals interactions.

MMX compounds of $A_4[Pt_2(pop)_4X]\cdot nH_2O$, especially Cl- and Br-bridged compounds, have been extensively studied by X-ray crystal structure analyses, Raman spectroscopy, and optical spectroscopy.[6] It has been found that electron−lattice interactions in these compounds are reduced following the order X = Cl > Br > I. However, all of the pop families discussed to this point have been semiconductors. Representing a different situation, compounds of $M_2(dta)_4I$ (M = Ni, Pt) were first prepared and characterized by Bellitto et al.[7] In $Ni_2(dta)_4I$, a sharp peak was observed at ~0.6 eV in the polarized reflectance spectrum parallel to the 1-D chain, which is due to the relatively large on-site Coulomb repulsion energy U of nickel atoms.[8a] Accordingly, this compound is regarded as a Mott−Hubbard semiconductor.[8a] Recently, the transport and spectroscopic studies of $Pt_2(dta)_4I$ by Kitagawa et al. revealed that a single crystal of this compound shows a high electrical conductivity of 13 S cm^{-1} at room temperature and exhibits metallic behavior above 300 K.[10] This result is particularly surprising considering that the half-filled 1-D band should lead to a semiconducting rather than to a metallic state due to on-site Coulomb repulsion U.[13] This is the first example of a metallic 1-D halogen-bridged transition metal complex. Furthermore, variable-temperature X-ray crystal structure analyses by Ozawa, Toriumi, et al. have revealed that $Pt_2(dta)_4I$ undergoes a structural phase transition near 372 K accompanying dynamic disorder of two PtS_4 planes, whereas the space group changes from $C2/c$ at low temperature to $A2/m$ at high temperature. Furthermore, the cell volume of the high-temperature phase is half that of the low-temperature one.[11] The dominant structural feature of $Pt_2(dta)_4I$ is a twisting

(5) (a) Nasu, K. *J. Phys. Soc. Jpn.* **1983**, *52*, 3865−3873. (b) Nasu, K. *J. Phys. Soc. Jpn.* **1984**, *53*, 302−311. (c) Toriumi, K.; Wada, Y.; Mitani, T.; Bandow, S.; Yamashita, J.; Fujii, Y. *J. Am. Chem. Soc.* **1989**, *111*, 2341−2342.

(6) (a) Che, C.-M.; Herbstein, F. H.; Schaefer, W. P.; Marsh, R. E.; Gray, H. B. *J. Am. Chem. Soc.* **1983**, *105*, 4604−4607. (b) Kurmoo, M.; Clark, R. J. H. *Inorg. Chem.* **1985**, *24*, 4420−4425. (c) Clark, R. J. H.; Kurmoo, M.; Dawes, H. M.; Hursthouse, M. B. *Inorg. Chem.* **1986**, *25*, 409−412. (d) Butler, L. G.; Zietlow, M. H.; Che, C.-M.; Schaefer, W. P.; Sridhar, S.; Grunthaner, P. J.; Swanson, B. I.; Clark, R. J. H.; Gray, H. B. *J. Am. Chem. Soc.* **1988**, *110*, 1155−1162. (e) Swanson, B. I.; Stroud, M. A.; Conradson, S. D.; Zietlow, M. H. *Solid State Commun.* **1988**, *65*, 1405−1409. (f) Stroud, M. A.; Drickamer, H. G.; Zietlow, M. H.; Gray, H. B.; Swanson, B. I. *J. Am. Chem. Soc.* **1989**, *111*, 66−72. (g) Jin, S.; Ito, T.; Toriumi, K.; Yamashita, M. *Acta Crystallogr., Sect. C* **1989**, *45*, 1415−1417. (h) Yamashita, M.; Toriumi, K. *Inorg. Chim. Acta* **1990**, *178*, 143−149. (i) Mitani, T.; Wada, Y.; Yamashita, M.; Toriumi, K.; Kobayashi, A.; Kobayashi, H. *Synth. Met.* **1994**, *64*, 291−294. (j) Kimura, N.; Ohki, H.; Ikeda, R.; Yamashita, M. *Chem. Phys. Lett.* **1994**, *220*, 40−45. (k) Wada, Y.; Furuta, T.; Yamashita, M.; Toriumi, K. *Synth. Met.* **1995**, *70*, 1195−1196. (l) Yamashita, M.; Miya, S.; Kawashima, T.; Manabe, T.; Sonoyama, T.; Kitagawa, H.; Mitani, T.; Okamoto, H.; Ikeda, R. *J. Am. Chem. Soc.* **1999**, *121*, 2321−2322.

(7) (a) Bellitto, C.; Flamini, A.; Gastaldi, L.; Scaramuzza, L. *Acta Crystallogr., Sect. A* **1981**, *37*, C172−C173. (b) Bellitto, C.; Flamini, A.; Gastaldi, L. Scaramuzza, L. *Inorg. Chem.* **1983**, *22*, 444−449. (c) Bellitto, C.; Dessy, G.; Fares, V. *Inorg. Chem.* **1985**, *24*, 2815−2820.

(8) (a) Yamashita, M.; Wada, Y.; Toriumi, K.; Mitani, T. *Mol. Cryst. Liq. Cryst.* **1992**, *216*, 207−212. (b) Shirotani, I.; Kawamura, A.; Yamashita, M.; Toriumi, K.; Kawamura, H.; Yagi, T. *Synth. Met.* **1994**, *64*, 265−270.

(9) (a) Kinoshita, S.; Wakita, H.; Yamashita, M. *J. Chem. Soc., Dalton Trans.* **1989**, 2457−2459. (b) Ikeda, R.; Kimura, N.; Ohki, H.; Furuta, T.; Yamashita, M. *Synth. Met.* **1995**, *71*, 1907−1908.

(10) (a) Kitagawa, H.; Onodera, N.; Ahn, J.-S.; Mitani, T.; Kim, M.; Ozawa, Y.; Toriumi, K.; Yasui, K.; Manabe, T.; Yamashita, M. *Mol. Cryst. Liq. Cryst.* **1996**, *285*, 311−316. (b) Kitagawa, H.; Onodera, N.; Ahn, J.-S.; Mitani, T.; Toriumi, K.; Yamashita, M. *Synth. Met.* **1997**, *86*, 1931−1932. (c) Kitagawa, H.; Mitani, T. *Coord. Chem. Rev.* **1999**, *190−192*, 1169−1184. (d) Kitagawa, H.; Onodera, N.; Sonoyama, T.; Yamamoto, M.; Fukawa, T.; Mitani, T.; Seto, M.; Maeda, Y. *J. Am. Chem. Soc.* **1999**, *121*, 10068−10080.

(11) Ozawa, Y.; Kim, M.; Takata, K.; Toriumi, K., manuscript to be submitted.

(12) Bray, J. W.; Interrante, L. V.; Jacobs, I. S.; Bonner, J. C. In *Extended Linear Chain Compounds*; Miller, J. S. Ed; Plenum Press: New York, 1983; Vol. 3, Chapter 7.

(13) Torrance, J. B. *Acc. Chem. Res.* **1979**, *12*, 79−86.

Table 1. Crystallographic Data for [Pt$_2$(EtCS$_2$)$_4$I$_2$] (**2**) and Pt$_2$(EtCS$_2$)$_4$I (**3**)

compound	**2**	**3**	**3**	**3**	**3**	**3**	**3**
formula	$C_{12}H_{20}I_2Pt_2S_8$	$C_{12}H_{20}IPt_2S_8$	$C_{12}H_{20}IPt_2S_8$	$C_{12}H_{20}IPt_2S_8$	$C_{12}H_{20}IPt_2S_8$	$C_{12}H_{20}IPt_2S_8$	$C_{12}H_{20}IPt_2S_8$
fw	1064.76	937.85	937.85	937.85	937.85	937.85	937.85
temp, K	296	115	149	184	252	293	377
cryst color	dark violet	black	black	black	black	black	black
cryst syst	monoclinic	monoclinic	monoclinic	monoclinic	monoclinic	monoclinic	monoclinic
space group	$P2_1/a$	$C2/c$	$C2/c$	$C2/c$	$C2/c$	$C2/c$	$C2/c$
a, Å	16.049 (2)	17.369 (2)	17.41 (1)	17.40 (1)	17.417 (4)	17.438 (5)	17.476 (3)
b, Å	11.062 (1)	8.590 (1)	8.602 (2)	8.610 (2)	8.639 (1)	8.644 (1)	8.666 (1)
c, Å	15.772 (2)	18.440 (3)	18.47 (1)	18.49 (1)	18.525 (4)	18.569 (6)	18.667 (3)
β, deg	117.132 (4)	125.317 (5)	125.31 (3)	125.22 (2)	125.14 (1)	125.05 (1)	125.004 (7)
V, Å^3	2491.9 (4)	2244. 9 (5)	2257 (2)	2263 (1)	2279.6 (8)	2291 (1)	2315.7 (6)
Z	4	4	4	4	4	4	4
D_{calc} g cm^{-3}	2.838	2.775	2.760	2.752	2.732	2.718	2.690
reflcns collcd	7851	3563	3584	3584	3614	7300	3677
unique reflcns	7603	3467	3488	3488	3517	7089	3580
reflcns used ($I > 3\sigma(I)$)	4560	2853	2665	2626	2575	2748	2568
R	0.033	0.026	0.031	0.031	0.036	0.026	0.027
R_W	0.038	0.040	0.047	0.048	0.053	0.034	0.035
goodness of fit	1.28	1.71	1.77	1.80	1.96	1.39	1.32

of two PtS_4 planes from an eclipsed arrangement characterized through the twist angle. This results from the S···S distance (~3.0 Å) of the SCS moiety being longer than the Pt−Pt distance (~2.68 Å).[7a,b,11] The two PtS_4 planes in Pt$_2$(dta)$_4$I are twisted with a twist angle of 21.4 ° in the low-temperature phase at room temperature,[7a,b] while dinuclear units in the high-temperature phase at 403 K adopt two staggered arrangements with twist angles of 19.4 and −19.4 °, respectively.[11] From consideration of molecular models, it is presumed that the twisting vibration of two PtS_4 planes would induce Pt−Pt and Pt−I stretching vibrations and further electron migration between diplatinum units. To clarify the anomalous structural and solid-state properties observed for Pt$_2$(dta)$_4$I, we have investigated the correlation between crystal structure and solid-state properties for chemically modified MMX chain compounds. If the interaction between 1-D chains were to be changed through chemical modification, drastic alteration in solid-state properties would be expected, as fluctuations of charge, spin, and lattice in a highly 1-D system play an important role in solid-state properties.

We have successfully synthesized a new MMX chain compound, Pt$_2$(EtCS$_2$)$_4$I (**3**), from [Pt$_2$(EtCS$_2$)$_4$] (**1**) and [Pt$_2$(EtCS$_2$)$_4$I$_2$] (**2**). We report here the syntheses, UV−visible−near-IR, IR, polarized Raman spectroscopy, and X-ray photoelectron spectroscopy (XPS) of these compounds, in addition to the X-ray crystal structure analyses of **2** and **3**. Compound **3** was further characterized by electrical transport measurements, determination of the temperature dependence of lattice parameters, X-ray diffuse scattering, determination of the temperature dependence of polarized Raman spectra, and SQUID magnetometry.

Experimental Section

Syntheses. Unless otherwise stated, all manipulations were performed at room temperature under argon atmosphere with standard vacuum line and Schlenk techniques. All solvents were dried using appropriate drying agents and freshly distilled under argon before use.[14] Dithiopropanoic acid, EtCS$_2$H,[15] bis(benzonitrile)dichloroplatinum(II), PtCl$_2$(NCPh)$_2$,[16] and Pt$_2$(dta)$_4$I[7b] were prepared according to published procedures. Elemental analyses were performed using a Perkin-Elmer 2400 series II CHNS/O analyzer.

[Pt$_2$(EtCS$_2$)$_4$] (1). To a solution of dithiopropanoic acid (1.95 g, 18.4 mmol) in 300 mL of toluene, PtCl$_2$(NCPh)$_2$ (2.16 g, 4.58 mmol) was added under an argon atmosphere. The mixture was refluxed for 2 h with stirring during which the solution turned dark red. On cooling, brownish olive needles with copper luster separated from the solution. These were collected and washed with toluene. The crude product was recrystallized from toluene to afford 1.41 g (71% yield based on PtCl$_2$(NCPh)$_2$) of **1** as brownish olive needles with copper luster. IR (KBr, cm^{-1}): 2978 (w), 2929 (w), 2910 (vw), 2868 (vw), 1456 (w), 1450 (w), 1425 (m), 1365 (w), 1298 (w), 1273 (w), 1157 (s), 1099 (vw), 1045 (m), 962 (s), 947 (m), 939 (m), 783 (vw), 615 (vw), 538 (w). Anal. Calcd for $C_{12}H_{20}Pt_2S_8$: C, 17.77; H, 2.49. Found: C, 17.77; H, 2.44.

[**Pt$_2$(EtCS$_2$)$_4$I$_2$] (2).** Compound **1** (488 mg, 0.601 mmol) was dissolved in 100 mL of toluene under reflux. To this strong reddish orange solution was added a solution of iodine (183 mg, 0.721 mmol) in 20 mL of toluene. On cooling, dark violet crystals with metallic luster separated from the resulting deep violet solution and were collected by suction filtration, washed with toluene, and dried in vacuo (yield 84%). IR (KBr, cm^{-1}): 2976 (m), 2929 (m), 2872 (m), 1450 (s), 1425 (w), 1398 (w), 1371 (m), 1325 (w), 1257 (w), 1155 (s), 1088 (m), 1041 (w), 985 (s), 957 (m), 943 (m), 762 (vw), 546 (vw). Anal. Calcd for $C_{12}H_{20}I_2Pt_2S_8$: C, 13.54; H, 1.89. Found: C, 13.59; H, 1.85.

Pt$_2$(EtCS$_2$)$_4$I (3). Compound **3** was prepared by a procedure similar to a literature method.[7b] Compounds **1** (27 mg, 0.033 mmol) and **2** (37 mg, 0.035 mmol) were dissolved in 15 mL of toluene at 110 °C, and the solution was heated for 15 additional minutes. On slow cooling, black plate crystals that separated from the resulting solution were collected by suction filtration and washed with toluene (55 mg, 89%). IR (KBr, cm^{-1}): 1456 (w), 1448 (w), 1431 (w), 1365 (w), 1284 (w), 1263 (vw), 1159 (w), 1142 (vw), 1103 (vw), 1022 (m), 964 (w), 945 (w), 933 (w), 617 (vw), 548 (vw). Anal. Calcd for $C_{12}H_{20}IPt_2S_8$: C, 15.37; H, 2.15. Found: C, 15.65; H, 2.11.

UV−Visible−Near-IR and IR Spectroscopy. UV−visible−near-IR spectra of the complexes as KBr pressed disks were recorded on a Hitachi U-3500 spectrophotometer equipped with a 60-mm-i.d. integrating-sphere apparatus. IR spectra were recorded as KBr pressed disks on a Horiba FT-200 spectrophotometer.

X-ray Crystal Structure Analyses. A summary of the crystallographic data and intensity data collection for all structures is given in Table 1. Crystallographic information files (CIF) for all data sets are listed in Supporting Information.

[Pt$_2$(EtCS$_2$)$_4$I$_2$] (2). A crystal with dimensions of 0.160 × 0.127 × 0.100 mm^3 was mounted on a glass fiber with epoxy resin. All measurements were made on an Enraf Nonius CAD4 diffractometer with graphite-monochromated Mo Kα radiation (λ = 0.710 69 Å) at

(14) Perrin, D. D.; Armarego, W. L. F. *Purification of Laboratory Chemicals*; Pergamon Press: New York, 1988.

(15) Hartke, K.; Rettberg, N.; Dutta, D.; Gerber, H.-D. *Liebigs Ann. Chem.* **1993**, 1081−1089.

(16) Anderson, G. K.; Lin, M. *Inorg. Synth.* **1990**, *28*, 60−63.

296 K. Accurate cell dimensions and crystal orientation matrixes were determined by least-squares refinement of 25 reflections in the range $24.93 < 2\theta < 29.77°$. The intensities of 7851 (7603 unique) reflections were collected to a maximum 2θ value of 59.9° by the $\theta-2\theta$ scan technique. A total of 4560 reflections with $I > 3\sigma(I)$ were used in structure refinement. Lorentz, polarization, and a numerical absorption correction were applied to the intensity data. The observed systematic absence of $h0l$ for $h = 2n + 1$ and $0k0$ for $k = 2n + 1$ led to the assignment of a monoclinic space group of $P2_1/a$. The structure was solved by direct methods[17] and expanded using Fourier techniques. All non-hydrogen atoms were refined anisotropically while all hydrogen atoms were placed at their idealized positions (C−H = 0.95 Å) and left unrefined. The full-matrix least-squares refinement based on 4560 observed reflections ($I > 3\sigma(I)$ and 217 variable parameters) converged to $R = 0.033$ and $R_W = 0.038$. The maximum and minimum peaks on the final difference Fourier map corresponded to 0.95 and −1.59 e^- Å^{-3}, respectively. All calculations were performed using the teXsan crystallographic software package from the Molecular Structure Corp.[18]

$Pt_2(EtCS_2)_4I$ (3). The temperature dependence of the lattice parameters of **3** as well as the intensity of reflections were measured on an Enraf Nonius CAD4 diffractometer with graphite-monochromated Mo Kα radiation ($\lambda = 0.710\,69$ Å), equipped with a Rigaku variable-temperature apparatus based on a cold nitrogen gas stream method. Crystals were mounted on glass fibers with epoxy resin. Lattice parameters in the temperature range of 105−390 K were determined based on 2θ values of 25 reflections with $25° < 2\theta < 30°$. Temperature adjustment of crystals was carried out at a rate of ∼0.3 K min^{-1}. Structure analyses were made at six temperatures, 115, 149, 184, 252, 293, and 377 K. The intensities of 3467 (115 K), 3488 (149 K), 3488 (184 K), 3517 (252 K), 7089 (293 K), and 3580 (377 K) reflections were collected to a maximum 2θ value of 59.9° by the $\theta-2\theta$ scan technique. A total of 2853 (115 K), 2665 (149 K), 2626 (184 K), 2575 (252 K), 2748 (293 K), and 2568 (377 K) intensities with $I > 3\sigma(I)$ were used for structure refinements. Lorentz, polarization, and a numerical absorption correction were applied to all intensity data. The observed systematic absence of hkl for $h + k = 2n + 1$ and $h0l$ for $l = 2n + 1$, being the same for all the data, led to two possible monoclinic space groups of *Cc* and *C*2/*c*. The latter was retained on the basis of the successful solution and refinement of the structure. All structures were solved by direct methods[17] and expanded using Fourier techniques. Non-hydrogen atoms were refined anisotropically while all hydrogen atoms were placed at their idealized positions (C−H = 0.95 Å) and left unrefined. The maximum and minimum peaks on the final difference Fourier maps correspond to 1.44 and −5.90 e^- Å^{-3} (115 K), 0.74 and −5.29 e^- Å^{-3} (149 K), 0.82 and −3.75 e^- Å^{-3} (184 K), 0.90 and −5.28 e^- Å^{-3} (252 K), 0.65 and −3.19 e^- Å^{-3} (293 K), and 0.63 and −3.10 e^- Å^{-3} (377 K). Large residual peaks are less than 2.0 Å from the Pt and I atoms. All calculations were performed using the teXsan crystallographic software package from the Molecular Structure Corp.[18]

X-ray Photoelectron Spectroscopy. XPS data were obtained using a VG Escalab MKII spectrometer equipped with a nonmonochromatized Mg Kα (1253.6 eV) X-ray source operated at 15 kV and 10 mA. Measurements were carried out in the 10^{-7} Pa pressure range. Samples were powdered and spread on conductive adhesive tape attached to sample holders. The absence of X-ray beam effects was checked by the X-ray power dependence of XPS spectra. The carbon 1s binding energy (284.6 eV) was used to calibrate the binding energy.[19] Curve-fitting analysis to determine binding energies and relative intensities was performed with an iterative least-squares computer program using a combination of Gaussian and Lorentzian line shapes to best fit the experimental envelope.

Electrical Transport Measurements. Dc electrical conductivity measurements of plate crystals of **3** along the *b* axis (1-D chain direction) were made on several single crystals in a temperature range of 80−400 K using a four-probe technique. Electrical contacts on the sample were made with gold paint to 25-μm-o.d. gold wires. The sample was placed in a liquid nitrogen cryostat with helium as the exchange gas in which temperature was monitored through a calibrated Si diode sensor located in close proximity to the sample.

The thermoelectric power of **3** was measured through a dynamical differential method using two sets of Au(Fe)−chromel thermocouples (76-μm o.d.). The temperature gradient across the plate crystal along the *b* axis was increased using a heater up to ∼0.5 K and simultaneously monitored by the thermocouples connected to separate nanovoltmeters. Absolute thermoelectric power was obtained after correction for the calibrated chromel.

X-ray Diffuse Scattering. X-ray diffraction photographs of **3** were taken in the temperature range of 90−325 K by a fixed-film and fixed-crystal method using synchrotron radiation at the SPring-8 BL02B1 station. The synchrotron radiation of 30.0 keV ($\lambda = 0.413$ Å) was monochromated by a Si(111) double-crystal monochromator and a pair of total reflection mirrors. The diffraction pattern was recorded with an exposure time of 30 min on an imaging plate (IP) area detector attached on a Huber seven-axes diffractometer, equipped with a Rigaku variable-temperature apparatus based on a cold nitrogen gas stream method. The distance from crystal to IP was 150 mm. Crystals with a typical size of 0.35 × 0.14 × 0.63 mm^3 were used. Oscillation photographs were also taken with the condition of an oscillation range of 8 ° and exposure time of 10 min in order to index weak superlattice reflections. The cell dimensions including superlattice reflections were determined by indexing all reflections including weak superlattice reflections using the DENZO program.[20]

Polarized Raman Spectra. Polarized Raman spectra were recorded with a Jasco NR-1800 subtractive-dispersion triple (filter single) polychromator using a microscope. A Spectra-Physics model 2017 Ar^+ laser provided the exciting line (514.5 nm). Detection of scattered radiation was made by a cooled Photometrics CC200 CCD camera system with an operating temperature of 153 K. Wavenumber calibration was made based on the Raman spectrum of indene, the emission lines of a Ne lamp, and plasma lines of an Ar^+ ion laser. Spectra were measured in the temperature range of 1.5−400 K using an Oxford Optista cryostat. Typical dimensions of single crystals of **1**−**3** were 0.10 × 0.10 × 0.50, 0.16 × 0.13 × 0.10, and 0.35 × 0.10 × 1.00 mm^3, respectively. The $Z(YY)\bar{Z}$ and $Z(XX)\bar{Z}$ components of the scattered radiation were used, where $X \parallel a + a$, $Y \parallel c$, and $Z \parallel a - a$ for **1**, $X \parallel b^*$ ($= b$), $Y \parallel a$, and $Z \parallel c^*$ for **2**, and $X \parallel a^* + c^*$, $Y \parallel b^*$, and $Z \parallel a^* - c^*$ for **3** (the 1-D chain $\parallel b^*$ ($= b$)).

Magnetic Susceptibility. Measurements were made using a Quantum Design MPMS-5 SQUID magnetometer in the temperature range of 2−400 K at a field of 1 T. Crystalline samples of **3** held in a Teflon film inside a plastic tube were used. Correction for core diamagnetism was made using the sum of the diamagnetism of **1** and half the Pascal constant of iodine.

Computational Methods. All the calculations based on density functional theory (DFT) were performed using the Gaussian 98 software package on a DEC-AXP-OSF/1 computer.[21] Input geometries of **1** and **2** were taken from the atomic coordinates determined by X-ray structure analyses for **1**[22] and **2**. All geometry optimizations and frequency

(17) Altomare, A.; Burla, M. C.; Camalli, M.; Cascarano, M.; Giacovazzo, C.; Guagliardi, A.; Polidori, G., *J. Appl. Crystallogr.* **1994**, *27*, 435.

(18) teXsan. Crystal Structure Analysis Package. Molecular Structure Corp., 1985 and 1992.

(19) *Handbook of X-ray Photoelectron Spectroscopy*; Wagner, C. D., Riggs, W. M., Davis, L. E., Moulder, J. F., Mullenberg, G. E., Eds.; Perkin-Elmer Corp.: Eden Prairie, MN, 1995.

(20) Otwinowski, Z.; Minor, W. *Methods Enzymol.* **1997**, *276*, 307−326.

(21) Frisch, M. J.; Trucks, G. W.; Schlegel, H. B.; Scuseria, G. E.; Robb, M. A.; Cheeseman, J. R.; Zakrzewski, V. G.; Montgomery, Jr., J. A.; Stratmann, R. E.; Burant, J. C.; Dapprich, S.; Millam, J. M.; Daniels, A. D.; Kudin, K. N.; Strain, M. C.; Farkas, O.; Tomasi, J.; Barone, V.; Cossi, M.; Cammi, R.; Mennucci, B.; Pomelli, C.; Adamo, C.; Clifford, S.; Ochterski, J.; Petersson, G. A.; Ayala, P. Y.; Cui, Q.; Morokuma, K.; Malick, D. K.; Rabuck, A. D.; Raghavachari, K.; Foresman, J. B.; Cioslowski, J.; Ortiz, J. V.; Stefanov, B. B.; Liu, G.; Liashenko, A.; Piskorz, P.; Komaromi, I.; Gomperts, R.; Martin, R. L.; Fox, D. J.; Keith, T.; Al-Laham, M. A.; Peng, C. Y.; Nanayakkara, A.; Gonzalez, C.; Challacombe, M.; Gill, P. M. W.; Johnson, B.; Chen, W.; Wong, M. W.; Andres, J. L.; Gonzalez, C.; Head-Gordon, M.; Replogle, E. S.; Pople, J. A. Gaussian 98, Revision A.6, Gaussian, Inc., Pittsburgh, PA, 1998.

(22) Mitsumi, M.; Yoshinari, T.; Ozawa, Y.; Toriumi, K. *Mol. Cryst. Liq. Cryst.* **2000**, *342*, 127−132.

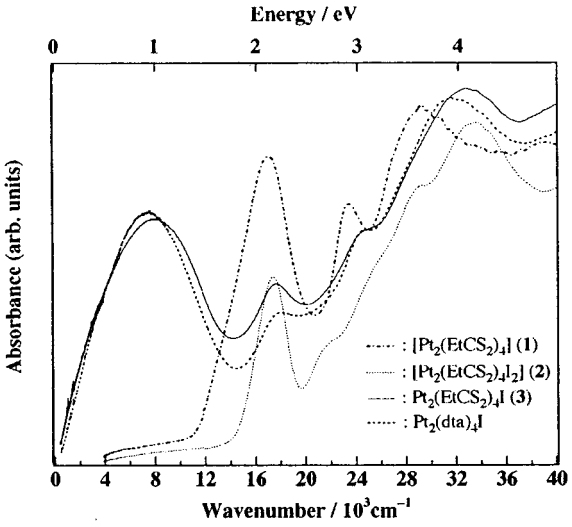

Figure 1. Electronic absorption spectra of $[Pt_2(EtCS_2)_4]$, $[Pt_2(EtCS_2)_4I_2]$, and $Pt_2(EtCS_2)_4I$ in the solid-state (KBr pressed disks), together with that of $Pt_2(dta)_4I$.

Table 2. Electronic Absorption Spectral Data of $[Pt_2(EtCS_2)_4]$ (**1**), $[Pt_2(EtCS_2)_4I_2]$ (**2**), and $Pt_2(EtCS_2)_4I$ (**3**) in the Solid State, Together with That of $Pt_2(dta)_4I$[a]

compd	wavenumber, 10^3 cm^{-1}
1	17.0, 23.4, 29.2
2	17.4, 21.8 (sh), 26.1 (sh), 29.2, 33.1
3	7.9, 17.7, 24.6 (sh), 33.0
$Pt_2(dta)_4I$	7.5, 17.9, 24.5 (sh), 31.8

[a] Measured as KBr pressed disks at 298 K. sh = shoulder.

calculations were performed at the B3LYP density functional theory level employing a LANL2DZ double-ζ basis set with no geometrical constraints.

Results and Discussion

Electronic Absorption Spectra. Electronic absorption spectra of $[Pt_2(EtCS_2)_4]$ (**1**), $[Pt_2(EtCS_2)_4I_2]$ (**2**), and $Pt_2(EtCS_2)_4I$ (**3**) are shown in Figure 1 in addition to spectrum for $Pt_2(dta)_4I$. Spectral data are summarized in Table 2.

The dominant feature of the absorption spectrum of **3** is an intense broad band centered at 7900 cm^{-1} (0.98 eV) that is absent from the spectra of **1** and **2**. This band is slightly shifted to higher energy relative to that of $Pt_2(dta)_4I$ (7500 cm^{-1} 0.93 eV). Highly conducting 1-D molecular-based conductors are known to show two intermolecular charge-transfer absorption bands, located at 7000−11 000 and 2000−4000 cm^{-1}.[23] For 7,7,8,8-tetracyanoquinodimethane (TCNQ) (A) salts ($\rho < 1$), the former is usually attributed to a charge-transfer (CT) transition of the type, $A^0A^{2-} \leftarrow A^-A^-$ (CT_1), and the latter to the $A^0A^- \leftarrow A^-A^0$ (CT_2) transition. The energy of CT_1 is largely determined by the Coulomb repulsion between electrons on the same molecule, while dc electrical conductivity is related to the low-energy CT_2 band. Since **3** has formally one unpaired electron per MMX unit, the lowest energy band can be attributed to the interdimer charge-transfer absorption CT_1, $d\sigma^{*0}d\sigma^{*2} \leftarrow d\sigma^{*1}d\sigma^{*1}$.[10d] This band extends to the infrared region; thus, relatively high electrical conductivity can be expected for **3**. The bands observed near 17 700 and 24 600 cm^{-1} for **3** are assigned to $d\sigma^* \leftarrow \sigma(I)$ and $d\sigma^* \leftarrow d\pi^*$ transitions, respectively, similar to assignment for $Pt_2(dta)_4I$.[10d] The absorption bands at 17 400 and 21 800 cm^{-1} in **2** are also attributable to $d\sigma^* \leftarrow \sigma(I)$ and $d\sigma^* \leftarrow d\pi^*$ transitions, respectively.[7b,24] The electronic absorption spectrum of **1** shows relatively intense bands at 17 000 and 23 400 cm^{-1}. The band at 17 000 cm^{-1}, however, disappears in solution. A similar electronic spectrum was observed for $[Pt_2(n\text{-}C_6H_{13}CS_2)_4]$ in the solid state in which the lowest energy band was assigned to a transition arising from electronic interactions between dinuclear units stacked in a linear fashion within the crystal.[25] Since similar stacking for **1** was revealed by X-ray analysis,[22] the bands at 17 000 cm^{-1} should have a similar origin. The band at 23 400 cm^{-1} could be assigned to the $p\sigma \leftarrow d\sigma^*$ transition by analogy with $[Pt_2(dta)_4]$[7b] and $[Pt_2(pop)_4]^{4-}$.[26]

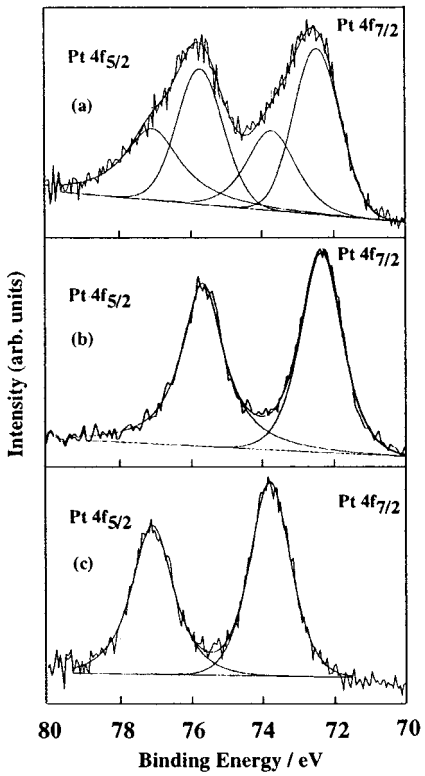

Figure 2. Pt $4f_{7/2}$ and $4f_{5/2}$ core level spectra for (a) **3**, (b) **1**, and (c) **2**.

X-ray Photoelectron Spectra. As will be described in detail later in the Transport Properties section, **3** undergoes the metal−semiconductor transition near 205 K. To examine valence states of the platinum atoms, the XPS of **3** was measured with those of **1** and **2**. The Pt $4f_{7/2}$ and $4f_{5/2}$ core level spectra for **1**−**3** at room temperature are shown in Figure 2. Binding energies of the Pt $4f_{7/2}$ and $4f_{5/2}$ core levels are summarized in Table 3. The Pt $4f_{7/2}$ and $4f_{5/2}$ peaks of **3** were broad compared to those of **1** and **2** and could be resolved into Pt^{2+} $4f_{7/2,5/2}$ and Pt^{3+}

(23) (a) Torrance, J. B.; Scott, B. A.; Kaufman, F. B. *Solid State Commun.* **1975**, *17*, 1369−1375. (b) Torrance, J. B.; Scott, B. A.; Welber, B.; Kaufman, F. B.; Seiden, P. E. *Phys. Rev. B* **1979**, *19*, 730−741. (c) Tanaka, J.; Tanaka, M.; Kawai, T.; Takabe, T. Maki, O. *Bull. Chem. Soc. Jpn.* **1976**, *49*, 2358−2373. (d) Torrance, J. B. In *Low-Dimensional Conductors and Superconductors*; Jérome, D., Caron, L. G., Eds.; NATO ASI Series, Series B; Plenum Press: New York, 1987; Vol. 155, pp 113−133. (e) Graja, A. In *Organic Conductors*; Farges, J.-P., Ed.; Marcel Dekker: New York, 1994; pp 229−267.

(24) (a) Bellitto, C.; Bonamico, M.; Dessy, G.; Fares, V.; Flamini, A. *J. Chem. Soc., Dalton Trans.* **1986**, 595−601.

(25) (a) Bellitto, C.; Flamini, A.; Piovesana, O.; Zanazzi, P. F. *Inorg. Chem.* **1980**, *19*, 3632−3636. (b) Bellitto, C.; Dessy, G.; Fares, V.; Flamini, A. *J. Chem. Soc., Chem. Commun.* **1981**, 409−411. (c) Bellitto, C.; Bonamico, M.; Dessy, G.; Fares, V.; Flamini, A. *J. Chem. Soc., Dalton Trans.* **1987**, 35−40. (d) Kawamura, T.; Ogawa, T.; Yamabe, T.; Masuda, H.; Taga, T. *Inorg. Chem.* **1987**, *26*, 3547−3550.

(26) Stiegman, A. E.; Rice, S. F.; Gray, H. B.; Miskowski, V. M. *Inorg. Chem.* **1987**, *26*, 1112−1116.

Table 3. XPS Data for $[Pt_2(EtCS_2)_4]$ (**1**), $[Pt_2(EtCS_2)_4I_2]$ (**2**), and $Pt_2(EtCS_2)_4I$ (**3**)

	binding energies, eV[a,b]			
compd	Pt^{2+} $4f_{7/2}$	Pt^{3+} $4f_{7/2}$	Pt^{2+} $4f_{5/2}$	Pt^{3+} $4f_{5/2}$
1	72.26 (1.39)		75.57 (1.39)	
2		73.74 (1.38)		77.05 (1.39)
3	72.41 (1.52)	73.68 (1.66)	75.69 (1.57)	77.04 (1.89)

[a] Full width at half-maximum values (fwhm) for peaks are given in parentheses. [b] These values were corrected against the C 1s peak using a value of 284.6 eV for C 1s peak.

$4f_{7/2,5/2}$ doublets using a curve resolver employing a Gaussian−Lorentzian line shape fit. The chemical shifts of each resolved doublet agreed well with those observed for **1** and **2**. It is apparent that **3** in the metallic state exists in the mixed-valence state composed of Pt^{2+} and Pt^{3+} on the time scale of XPS spectroscopy ($\sim 10^{-17}$ s). This result is consistent with data obtained for $Pt_2(dta)_4I$ by Kitagawa et al.[10c,d] The intensity of the Pt^{3+} $4f_{7/2,5/2}$ doublet is weak relative to that of Pt^{2+}. This may be due to reduction of Pt^{3+} to Pt^{2+} by X-ray irradiation.

Transport Properties. As will be described in detail later in the Crystal Structure section, **3** consists of a neutral 1-D chain with a repeating −Pt−Pt−I− unit. Single-crystal electrical conductivity along the 1-D chain was measured for several samples of **3**. As expected from analysis of the electronic absorption spectrum, **3** shows relatively high electrical conductivity (5−30 S cm^{-1}) at room temperature, comparable with that reported for $Pt_2(dta)_4I$ ($\sim$13 S cm^{-1}).[10] These values are 10^4 times greater than that of $K_4[Pt_2(pop)_4Br]\cdot 3H_2O$[6d] but are $\sim$10 times lower than that found in $K_2Pt(CN)_4Br_{0.3}\cdot 3H_2O$ (KCP(Br)).[27] Temperature dependence of the electrical resistivity of crystal **3** along the 1-D chain is represented in Figure 3. On decreasing temperature, the electrical resistivity increases, achieving a maximum around 235 K preceding a decrease to a minimum at 205 K. Below 205 K, the electrical resistivity behaves as a thermally activated semiconductor with an activated energy of 110 meV. The resistivity jump observed at 153 K upon cooling may be a result of microcracks within the crystal as such an anomaly was not observed upon heating.

Electrical conductivity above $\sim$200 K follows neither thermally activated nor typical metallic behavior. To determine whether electrical conducting behavior is metallic or not, the thermoelectric power *S* has been measured within the temperature range of 125−402 K (Figure 4). Above room temperature, *S* takes the temperature-independent small negative value, −15 μV K^{-1}. Upon cooling, *S* slightly increases and exhibits a slight swelling around 260−205 K before changing sign and increasing rapidly. In a 1-D tight-binding picture, the temperature dependence of *S* is given by

$$S = -\frac{\pi^2 k_B{}^2 T}{6|e||t|}\frac{\cos\left(\frac{1}{2}\pi\rho\right)}{1-\cos^2\left(\frac{1}{2}\pi\rho\right)} \qquad (1)$$

where *e* is the electron charge, ρ is the electron density in the band ($\rho = 1$ for one electron per site), and *t* is the transfer integral ($4t$ being the bandwidth *W*).[28] If MMX units form a metallic band, it will be an effective half-filled band mainly

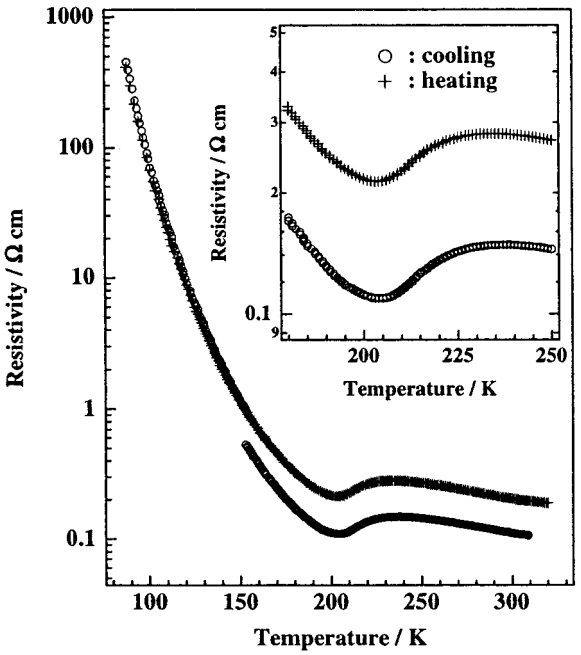

Figure 3. Temperature dependence of electrical resistivity measured along the chain axis *b* of **3**.

composed of the Pt−Pt dσ*−I p_z combination as the present compound has formally one unpaired electron per MMX unit. Within the tight-binding approximation, the thermoelectric power of the half-filled band ($\rho = 1$) would give a temperature-independent value of zero. The observed temperature-independent behavior of *S* above room temperature should correspond to MMX chain with an effective half-filled metallic band. The finite value of *S* may originate from a scattering of conduction electrons. Below 205 K, *S* changes its sign and increases rapidly with decreasing temperature. This drastic change in *S* observed near 205 K suggests an energy gap at the Fermi energy is opened below 205 K. The thermoelectric power for a semiconductor can be approximated using Boltzmann theory by

$$S = -\frac{k_B{}^2}{|e|}\left(\frac{b-1}{b+1}\frac{E_g}{kT} + \ln\frac{m_h}{m_e}\right) \qquad (2)$$

where *b* is the ratio of electron mobility to hole one ($b = \mu_e/\mu_h$) and m_h and m_e are the effective mass of the holes and electrons, respectively.[28] As seen in eq 2, thermoelectric power is inversely proportional to temperature. Below the transition temperature, the thermoelectric power of **3** varies approximately as $1/T$, suggesting a semiconducting state. These results indicate that **3** undergoes a metal−semiconductor transition at T_{M-S} = 205 K. The transition phenomena observed through electrical resistivity and thermoelectric power measurements are completely reversible and show no hysteresis.

In general, the 1-D metal undergoes a metal−semiconductor transition at higher temperature owing to the instability of the planar Fermi surface, but the transition temperature decreases upon increasing dimensionality.[29] Kitagawa et al. reported that $Pt_2(dta)_4I$ undergoes a metal−semiconductor transition at 300 K.[10c,d] Compound **3** has no interchain S···S contact, in contrast to $Pt_2(dta)_4I$, which has relatively short interchain S···S distances. However, it is surprising that the transition temperature of **3** is lower by $\sim$100 K than that of $Pt_2(dta)_4I$.

(27) Zeller, H. R.; Beck, A. *J. Phys. Chem. Solids* **1974**, *35*, 77−80.
(28) (a) Kwak, J. F.; Beni, G.; Chaikin, P. M. *Phys. Rev. B* **1976**, *13*, 641−646. (b) Chaikin, P. M.; Greene, R. L.; Etemad, S.; Engler, E. *Phys. Rev. B* **1976**, *13*, 1627−1632. (c) Chaikin, P. M. In *The Physics and Chemistry of Low Dimensional Solids*; Alcácer, L., Ed.; NATO ASI Series; D. Reidel Publishing: Dordrecht, The Netherlands, 1980; Vol. 56, pp 53−75.
(29) Kagoshima, S.; Nagasawa, H.; Sambongi, T. *One-Dimensional Conductors*; Springer Series in Solid-State Sciences; Springer-Verlag: Berlin, 1988; Vol. 72, Chapter 2.

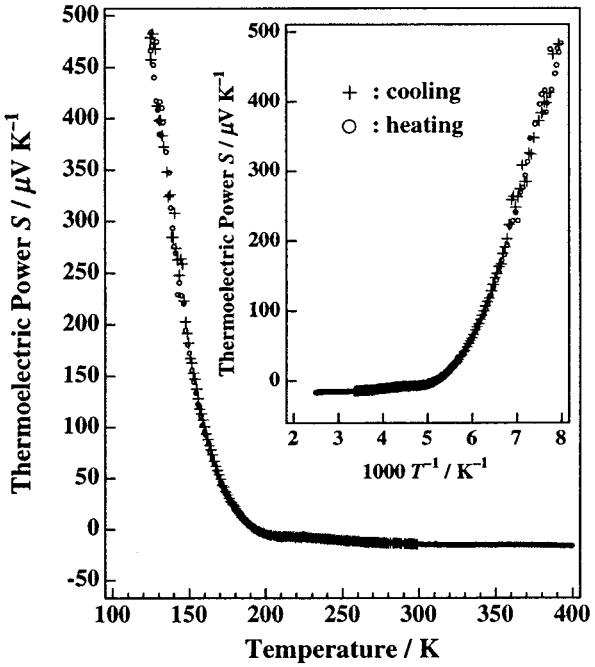

Figure 4. Temperature dependence of absolute thermoelectric power measured along the chain axis *b* of **3**.

The 1-D half-filled band of molecular-based conductors generally does not lead to metallic conduction if the on-site Coulomb repulsion *U* is large in comparison with the bandwidth *W*.[13] Recently, however, it has been reported that highly conductive 1:1 radical cation salts, (TTM−TTP)I_3 and DMTSA·BF_4, where TTM−TTP is 2,5-bis[4,5-bis(methylthio)-1,3-dithiol-2-ylidene]-1,3,4,6-tetrathiapentalene and DMTSA is 2,3-dimethyltetraselenoanthracene, show metallic conducting behavior down to 160 and 150 K, respectively, although they have half-filled energy bands.[30] The *U*/*W* parameters for these compounds were estimated to be ∼0.8. Small values of *U*/*W* are considered to be highly correlated with metallic conductivity at high temperature. The *U* of the MMX compound can be estimated to be small as two platinum atoms share one unpaired electron. Consequently, the metallic behavior of **3** is reasonable.

Crystal Structure of [Pt$_2$(EtCS$_2$)$_4$I$_2$] (2). The ORTEP diagram of **2** is shown in Figure 5. Selected bond distances of **2** are listed in Table 4. Compound **2** crystallizes in the monoclinic space group $P2_1/a$. The crystal consists exclusively of a neutral dinuclear $Pt^{3+}-Pt^{3+}$ complex, [Pt$_2$(EtCS$_2$)$_4$I$_2$], which sits on a general position. Two platinum atoms of the complex are bridged by four dithiopropanato ligands, $EtCS_2^-$. Each platinum atom is six coordinated in a tetragonally distorted octahedral geometry, surrounded by four sulfur atoms in an approximately square-planar arrangement with an iodine atom and the other platinum atom in the apical positions. The two PtS_4 planes are twisted with a twist angle of ∼26.9 ° from the eclipsed D_{4h} structure. The Pt−Pt distance of 2.582 (1) Å is 0.205 Å shorter than the distance between the mean planes defined by the four sulfur atoms. The Pt−Pt distance is considerably shorter than those observed in dinuclear $Pt^{2+}-Pt^{2+}$ (d^8d^8) compounds [Pt$_2$(dta)$_4$] (2.767 (1) Å)[25a] and **1** (2.764 (1) Å)[22] but is comparable to those observed in dinuclear $Pt^{3+}-Pt^{3+}$ (d^7d^7) compounds [Pt$_2$(Me$_2$CHCS$_2$)$_4$I$_2$]·I$_2$ (2.578 (1) Å) and [Pt$_2$(PhCH$_2$CS$_2$)$_4$I$_2$] (2.598 (2) Å).[24] The two Pt−I distances (2.766 (1) and 2.762 (1) Å) are nearly identical and are similar to those observed in [Pt$_2$(Me$_2$CHCS$_2$)$_4$I$_2$]·I$_2$ (average 2.764 Å) and [Pt$_2$(PhCH$_2$CS$_2$)$_4$I$_2$] (2.753 (3) Å).[24] The Pt−Pt−I angles are almost 180°, indicating linearity of the I−Pt−Pt−I sequence. The mean Pt−S distance and Pt−Pt−S angle are 2.339 (5) Å and 92.5 (2)°, respectively.

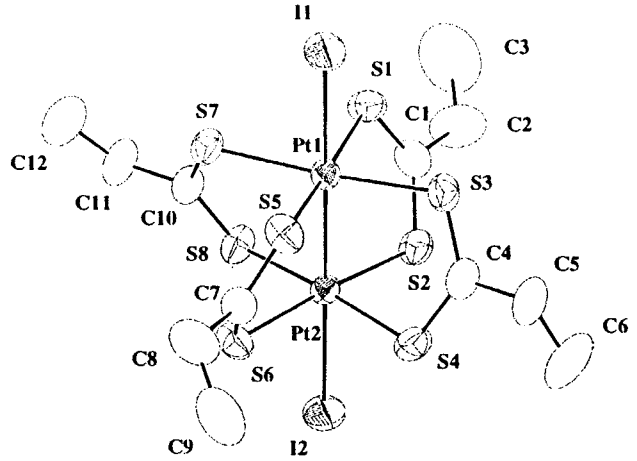

Figure 5. ORTEP diagram of **2** with atomic numbering scheme and 50% thermal ellipsoids.

Table 4. Selected Bond Distances (Å) with Esd's in Parentheses for [Pt$_2$(EtCS$_2$)$_4$I$_2$] (**2**)

bond	distance	bond	distance
Pt(1)−Pt(2)	2.582(1)	Pt(1)−I(1)	2.766(1)
Pt(1)−S(1)	2.346(2)	Pt(1)−S(3)	2.333(2)
Pt(1)−S(5)	2.335(2)	Pt(1)−S(7)	2.342(2)
Pt(2)−I(2)	2.762(1)	Pt(2)−S(2)	2.336(2)
Pt(2)−S(4)	2.342(2)	Pt(2)−S(6)	2.340(2)
Pt(2)−S(8)	2.333(2)		

Crystal Structure of Pt$_2$(EtCS$_2$)$_4$I (3). To elucidate the nature of structural modification brought about by the metal−semiconductor transition, single-crystal X-ray structure analyses have been performed at five temperatures below and above the transition at 205 K (115, 149, 184, 252, and 293 K). It has been found from differential scanning calorimetric measurements (DSC) that Pt$_2$(dta)$_4$I shows exothermic and endothermic peaks around 371−372 K corresponding to a first-order phase transition.[11] From crystal structure analyses of Pt$_2$(dta)$_4$I above and below the transition, it has been revealed that the dinuclear units adopt two staggered arrangements with twist angles of 19.4 and −19.4°, respectively, at high temperature.[11] However, DSC measurements of **3** do not show any latent heat in the temperature range of 150−473 K. To confirm that **3** does not exhibit positional disorder of the two PtS_4 planes, X-ray analysis has also been carried out at 377 K. ORTEP diagrams of **3** are shown in Figure 6. The stereoview of the unit cell at 293 K is shown in Figure 7 while selected bond distances are listed in Table 5.

3 crystallizes in the monoclinic space group $C2/c$, adopting a space group identical to that of the low-temperature phase of Pt$_2$(dta)$_4$I.[7a,b,11] The crystal consists of a neutral 1-D chain with a repeating −Pt−Pt−I− unit lying on the crystallographic 2-fold axis parallel to the *b* axis. Two platinum atoms are bridged by four dithiopropanato ligands with a Pt−Pt distance of 2.684 (1) Å at 293 K, 0.189 Å shorter than the distance between the mean

(30) (a) Mori, T.; Kawamoto, T.; Yamaura, J.; Enoki, T.; Misaki, Y.; Yamabe, T.; Mori, H.; Tanaka, S. *Phys. Rev. Lett.* **1997**, *79*, 1702−1705. (b) Mori, T.; Inokuchi, H.; Misaki, Y.; Yamabe, T.; Mori, H.; Tanaka, S. *Bull. Chem. Soc. Jpn.* **1994**, *67*, 661−667. (c) Tajima, H.; Arifuku, M.; Ohta, T.; Mori, T.; Misaki, Y.; Yamabe, T.; Mori, H.; Tanaka, S. *Synth. Met.* **1995**, *71*, 1951−1952. (d) Dong, J.; Yakushi, K.; Takimiya, K.; Otsubo, T. *J. Phys. Soc. Jpn.* **1998**, *67*, 971−977. (e) Takimiya, K.; Ohnishi, A.; Aso, Y.; Otsubo, T.; Ogura, F.; Kawabata, K.; Tanaka, K.; Mizutani, M. *Bull. Chem. Soc. Jpn.* **1994**, *67*, 766−772.

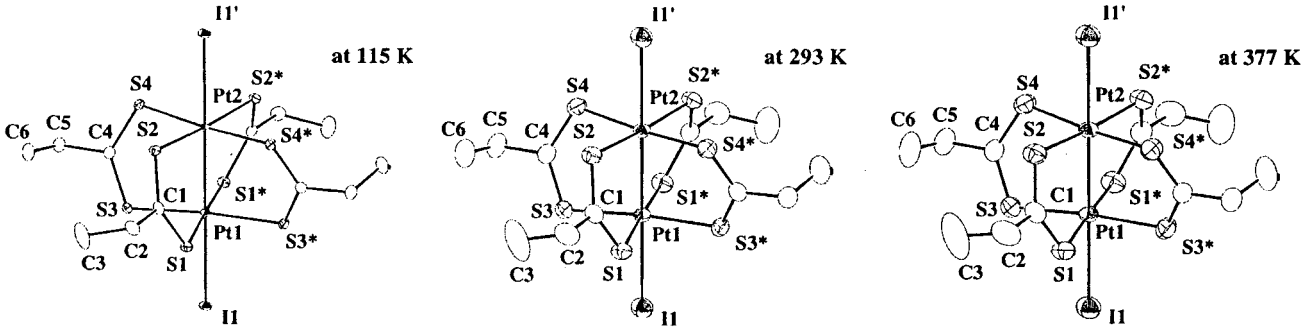

Figure 6. ORTEP diagrams of **3** at 115, 293, and 377 K with atomic numbering scheme and 50% thermal ellipsoids.

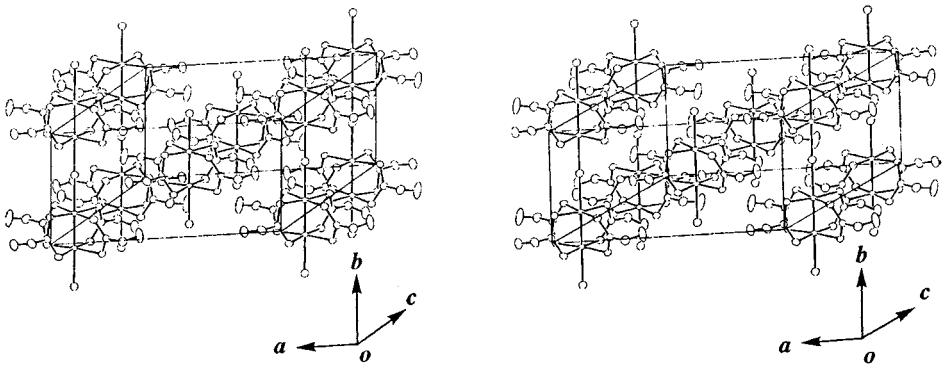

Figure 7. Stereoview of the unit cell of **3** at 293 K.

Table 5. Selected Bond Distances (Å) with Esd's in Parentheses for $Pt_2(EtCS_2)_4I$ (**3**) [a]

	temperature, K					
	115	149	184	252	293	377
Pt(1)−Pt(2)	2.680(1)	2.681(1)	2.682(1)	2.683(1)	2.684(1)	2.686(1)
Pt(1)−I(1)	2.957(1)	2.961(1)	2.964(1)	2.978(1)	2.982(1)	2.992(1)
Pt(1)−S(1)	2.333(1)	2.334(2)	2.336(2)	2.333(2)	2.332(1)	2.333(2)
Pt(1)−S(3)	2.323(1)	2.328(2)	2.324(2)	2.323(2)	2.322(1)	2.322(2)
Pt(2)−I(1)′	2.954(1)	2.960(1)	2.964(1)	2.978(1)	2.978(1)	2.989(1)
Pt(2)−S(2)	2.327(1)	2.329(2)	2.329(2)	2.325(2)	2.327(1)	2.326(2)
Pt(2)−S(4)	2.334(1)	2.336(2)	2.335(2)	2.332(2)	2.330(1)	2.332(2)

[a] Prime as superscript refers to the following equivalent positions relative to the *x*, *y*, *z* set: $+x, -1+y, +z$.

planes defined by the four sulfur atoms. This Pt−Pt distance is intermediate between that of the dinuclear $Pt^{2+}-Pt^{2+}$ (d^8d^8) **1** (2.764 (1) Å)[22] and the dinuclear $Pt^{3+}-Pt^{3+}$ (d^7d^7) **2** (2.582 (1) Å) and is nearly equal to that of $Pt_2(dta)_4I$ (2.677 (2) Å).[7a,b] This is consistent with the fact that the bond order of the Pt−Pt bond in **3** (d^8d^7) is formally $^1/_2$. Pt−I distances are 2.982 (1) and 2.978 (1) Å, respectively. These Pt−I distances are longer than those observed in **2** (average 2.764 Å) and are similar to those in $Pt_2(dta)_4I$ (average 2.978 Å).[7a,b] As shown in Table 5, the bridging iodine atom is located at the midpoint between dinuclear units within the experimental error at any temperature. Accordingly, the valence states of platinum atoms cannot be distinguished solely from crystal structure analysis. The two PtS_4 planes of the dinuclear unit are twisted by ~23.0 ° at 293 K from the eclipsed D_{4h} structure. Twist angles at 115 and 377 K were found to be about 24.0 and 22.5°, respectively. The twist angle slightly decreases with lengthening of the Pt−Pt distance. The positional disorder of PtS_4 planes that has been observed for $Pt_2(dta)_4I$ in the high-temperature phase[11] is not observed for **3**.

The temperature dependence of the Pt−Pt and Pt−I distances are shown in Figure 8. Linearly lengthening with increasing temperature, the Pt−Pt distance lengthens by 0.006 Å from 115 to 377 K. On the other hand, the average Pt−I distance increases discontinuously near the transition temperature and increases by 0.035 Å from 115 to 377 K. The increase in the Pt−I distance is remarkably larger than those observed for Pt−Pt and Pt−S

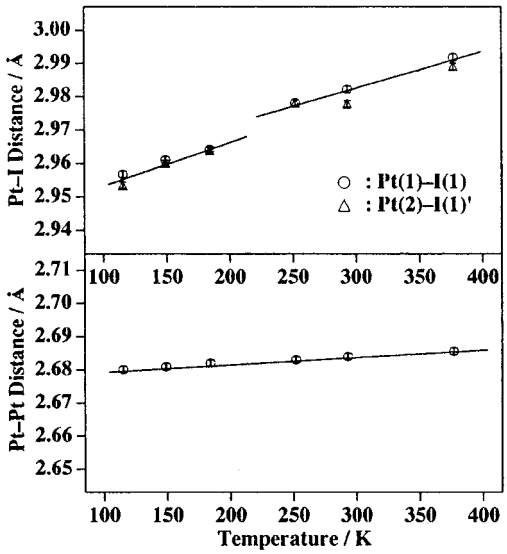

Figure 8. Temperature dependence of the Pt−Pt and Pt−I distances of **3**. Prime as superscript refers to the following equivalent positions relative to the x, y, *z* set: $+x, -1+y, +z$.

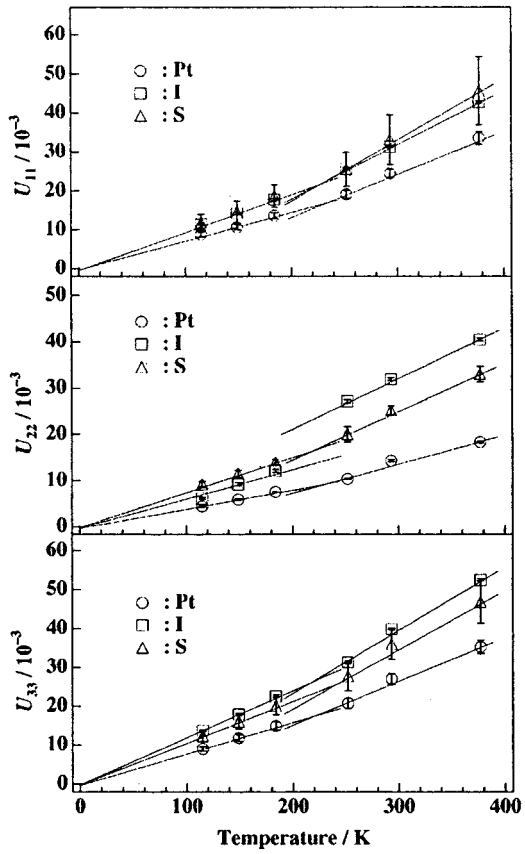

Figure 9. Temperature dependence of the average temperature factors, U_{11}, U_{22}, and U_{33} of Pt, I, and S atoms of **3**.

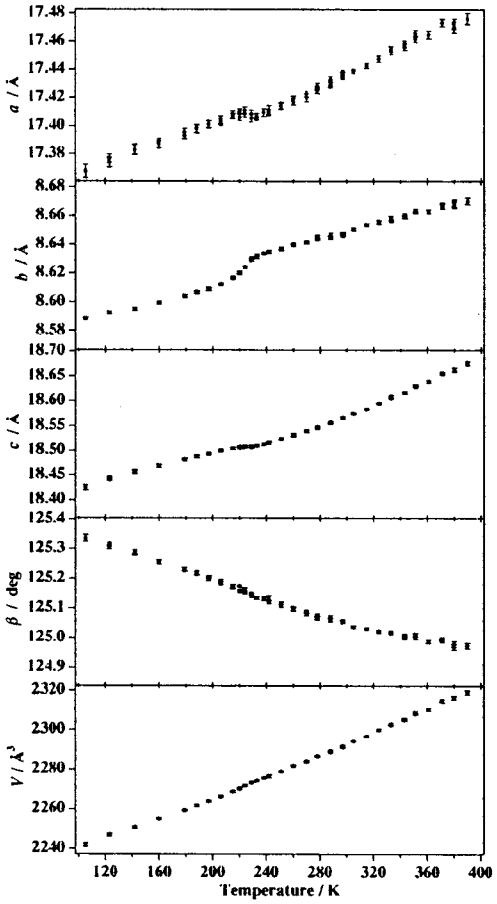

Figure 10. Temperature dependence of the lattice parameters of **3**.

distances. The average temperature factors, U_{11}, U_{22}, and U_{33} of Pt, I, and S atoms, respectively, are plotted against temperature in Figure 9. The temperature factor U, which corresponds to the mean square displacement of an atom from its mean position, can be expressed as $k_BT/\bar{\omega}_j^2$ for a classical harmonic oscillator at a temperature above the Einstein temperature.[31] As shown in Figure 9, U_{ii} for each atom increases linearly with temperature over each temperature region below or above T_{M-S}. However, it should be noted that the temperature dependence of U_{ii} for each atom changes around T_{M-S}. A more striking feature is the exceptionally steep increase in U_{22} of the bridging iodine atom around T_{M-S}, while the temperature dependence of U_{11} and U_{33} of the iodine atom changed slightly but continuously at T_{M-S}. This strongly suggests the iodine atom is positionally disordered or vibrates with a large amplitude in a smooth potential surface as temperature factors along the bond direction for atoms bound to each other are well predicted based on the rigid body approximation for molecular crystals. This phenomenon is consistent with large increases in the Pt−I distance and also with rapid increases in the lattice parameter *b* around T_{M-S}, which will be discussed in the following section.

As shown in Figure 7, neighboring 1-D chains along the *a* axis related by the *C* lattice are shifted by 0.5*b* analogously to the structure of $Pt_2(dta)_4I$ at low temperature. Adjacent 1-D chains along the *c* axis are related by a *c* glide plane while the two PtS_4 planes of diplatinum units in the neighboring 1-D chains twist in opposite directions. It is noteworthy that the overlapping mode between neighboring 1-D chains along *c* of **3** is different from that of $Pt_2(dta)_4I$. Neighboring chains along *c* are shifted by ~0.5*b* in $Pt_2(dta)_4I$, but are shifted by only 0.444 Å (293 K) in **3**. This shift slightly decreases with increasing temperature, 0.465 Å at 115 K and 0.428 Å at 377 K.

The distances of interchain S···S contacts are 3.812 and 3.847 Å in $Pt_2(dta)_4I$, similar to the van der Waals distance between sulfur atoms (3.60 Å).[7a,b] However, interchain S···S distances in **3** are found to be S(1)···S(1) ($^1/_2 - x$, $^1/_2 - y$, $1 - z$) = 4.140 (2) Å and S(2)···S(2) ($^1/_2 - x$, $-^1/_2 - y$, $1 - z$) = 4.663 (2) Å, indicating no interchain S···S contact. Interchain distances along the *a* and *c* directions in **3** are 8.719 and 9.285 Å, respectively, lengthened by 0.300 and 2.467 Å, in comparison with those of $Pt_2(dta)_4I$.

Temperature Dependence of Lattice Parameters. The lattice parameters *a*, *b*, *c*, β, and *V* of **3** were determined by X-ray diffraction experiments and are plotted as functions of temperature in Figure 10. These lattice parameters exhibit significant temperature dependence with drastic changes in slope at about 205−240 K, especially evident for parameter *b*. This is consistent with the metal−semiconductor transition as described in the Transport Properties section.

The temperature dependence of the lattice parameter *b* for temperature ranges above 240 K and below 205 K can each be well fit by straight lines. Linear thermal expansions ($\alpha_i = (dl_i/dT)/l_i$) are evaluated (in K^{-1}) as follows: $\alpha_b = 2.85 \times 10^{-5}$ at 297 K and 2.70×10^{-5} at 160 K. There is an obvious gap between two lines at 205−240 K. The steep change of lattice parameter *b* observed from 205 to 240 K can be evaluated from the difference between two extrapolated values of *b* as 0.015 Å. It is apparent from crystal structure analyses that the remarkable expansion of *b* is a result of the significant elongation of the Pt−I distance and of the drastic increase in U_{22} of I along the chain direction. The temperature dependence

(31) Bürgi, H. B.; Capelli, S. C. *Acta Crystallogr.* **2000**, *A56*, 403−412.

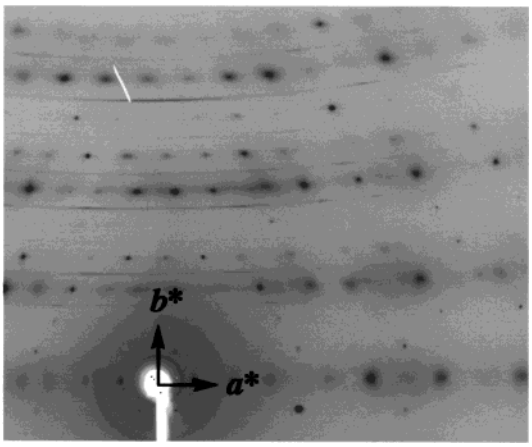

Figure 11. X-ray diffraction photograph of **3** taken with a fixed-film and fixed-crystal method at 297 K. The sample is oriented as the *a** and *b** directions perpendicular to the incident X-ray beam. *b** is vertical in this photograph.

of *a*, *c*, and *V* is almost linear in the temperature ranges above 240 K and below 205 K, while anomalous behaviors are found in the range 205−240 K. The linear thermal expansion coefficients (in K^{-1}) are as follows: $\alpha_a = 2.68 \times 10^{-5}$, $\alpha_c = 6.09 \times 10^{-5}$, and $\alpha_V = 1.28 \times 10^{-4}$ at 297 K; $\alpha_a = 2.01 \times 10^{-5}$, $\alpha_c = 3.65 \times 10^{-5}$, and $\alpha_V = 1.02 \times 10^{-4}$ at 160 K. The principal intermolecular interactions along the *a* and *c* directions can be regarded as van der Waals contacts among the 1-D chains, which should be weaker than those of the Pt−Pt or Pt−I bonds along the 1-D chains. Accordingly, the anomalous behavior of the lattice parameters *a*, *c*, and *V* observed between 205 and 240 K may be followed by the steep slope of *b*.

X-ray Diffuse Scattering. As previously described in the Crystal Structure section, the bridging iodine atom is located at the midpoint between two diplatinum units. This indicates valence states of the platinum atoms of **3** are considered to be an averaged valence state of +2.5. However, the XPS spectrum of **3** revealed that the diplatinum complex adopted the Pt^{2+}−Pt^{3+} mixed-valence state. It is well known that X-ray crystal structure analysis gives only a time and spatially averaged structure. On the other hand, **3** is expected to exhibit structural distortion even in the metallic state, since the 1-D halogen-bridged mixed-valence platinum complex is a typical system having strong electron−lattice interactions. X-ray diffuse scattering techniques are used to examine subtle periodic lattice distortion.[32] To obtain the crystal structure of **3**, including the periodical arrangement of platinum valences on the 1-D chain system, X-ray diffuse scattering was measured.

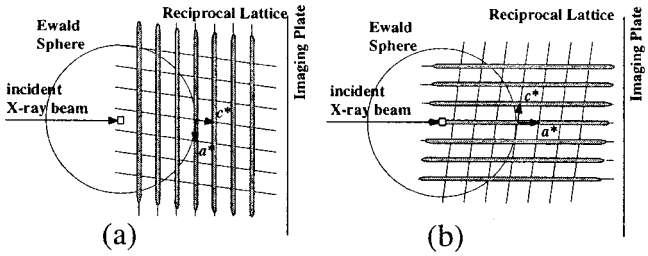

Figure 13. Schematic representations of the diffuse lines (−, $n + 0.5$, *l*) (*n*; integer) on a projection plane perpendicular to the *b** axis with the Ewald sphere. The sample is oriented as (a) the *a** and *b** directions perpendicular to the incident X-ray beam (same orientation as Figure 12a) and (b) the *b** direction perpendicular to the incident beam and the *a** parallel to it (same as Figure 12b).

The X-ray diffraction photographs taken on the different reciprocal planes between 206 and 297 K are shown in Figures 11 and 12. As shown in Figures 11 and 12a, the X-ray diffraction pattern exhibits weak but sharp diffuse lines at the midpoint between layers of Bragg reflections, i.e., at the reciprocal lattice positions in $k = n + 0.5$ (*n*; integer). On the other hand, the diffraction pattern in Figure 12b exhibits distinct spots on diffuse lines. Considering both diffraction patterns, it can be determined that the diffuse lines are extended perpendicular to the *b** axis (= chain axis *b*) and parallel to the *a** axis and are indexed as (−, $n + 0.5$, *l*) and shown in Figure 13. This implies that new periodic ordering with 2-fold repetition length of the MMX unit exists in the 1-D chain and that these structures are strongly coupled with each other along the *c* direction, resulting in 2-D order in the *bc* plane. The diffuse lines corresponding to 2-D ordering stand in contrast to the diffuse planes (1-D ordering) observed for the metallic state of 1-D conductors of KCP(Br)[33a,b] and TTF−TCNQ (TTF = tetrathiafulvalene).[33c−e]

The intensity of diffuse scattering increases with increasing scattering angles as shown in Figure 11. This strongly suggests that diffuse scattering arises from a displacive modulation of heavy atoms, i.e., static or dynamic distortion of the platinum or iodine positions. When the electron density ρ per unit cell with lattice constant *b* is 1, the Fermi wavenumber of the electron is $k_F = \rho b^*/4 = b^*/4$, where $b^* = 2\pi/b$ is the reciprocal lattice vector. Consequently, the reciprocal lattice vector $0.5b^*$

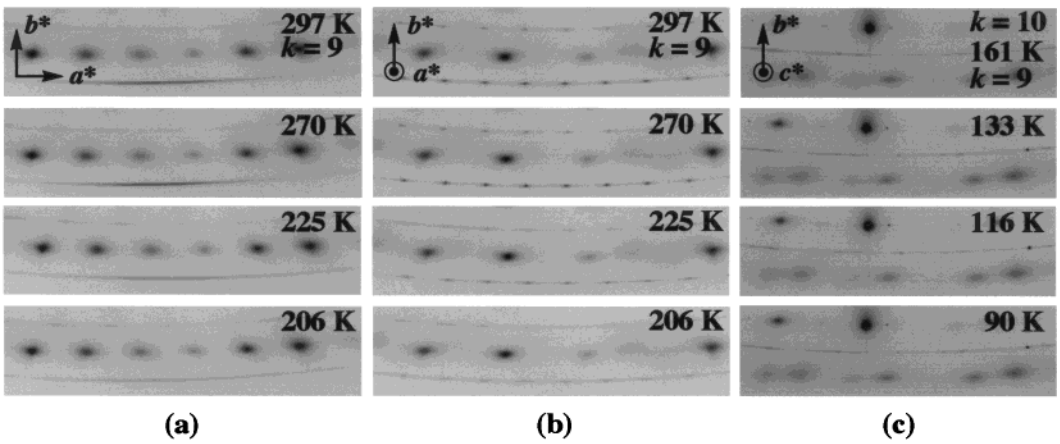

Figure 12. Portions of X-ray diffraction photographs of **3** taken at different temperatures and crystal orientations with a fixed-film and fixed-crystal method. *b** is vertical in these figures. The sample is oriented as (a) the *a** and *b** directions perpendicular to the incident X-ray beam, (b) the *b** direction perpendicular to the incident X-ray beam and the *a** direction parallel to it, and (c) the *b** direction perpendicular to the incident X-ray beam and the *c** direction parallel to it.

coincides with the $2k_F$ wave vector. This suggests that periodic ordering with 2-fold repetition length of the MMX units can be represented by $-Pt^{2+}-Pt^{2+}-I-Pt^{3+}-Pt^{3+}-I-$ ($2k_F$-CDW) or $-Pt^{2+}-Pt^{3+}-I-Pt^{3+}-Pt^{2+}-I-$ ($2k_F$). Diffuse scattering observed at $0.5b^*$ in the metallic region also indicates band gap opening at the Fermi level. Many physical properties of 1-D metal KCP(Br) were successfully explained based on a simple 1-D band model.[34,35] However, the $Pt^{2+}-Pt^{4+}$ mixed-valence state revealed by the XPS spectrum could not be explained by such a simple 1-D band model,[36] but was well interpreted using the valence fluctuation model.[35,37] Considering diffuse scattering observed for **3**, we believe that the platinum atoms in the metallic state of **3**, though in a valence fluctuating state, adopt periodic ordering with a 2-fold repetition length of the MMX units.

The diffuse lines are almost constant in intensity above 252 K; however, their intensity decreases progressively with decreasing temperature below 252 K accompanied by gradual changes in shape from lines to continuous sheets around T_{M-S}. This indicates that the periodic ordering of the MMX units changes from 2-D to 1-D. This transformation in the dimensionality of valence ordering should be associated with a drastic change in the chain axis b around T_{M-S}. As shown in Figures 12c and 14, broad undulation in the intensity of the diffuse sheets gradually converts to weak but distinct Bragg spots corresponding to superlattice reflections around temperatures between 161 and 133 K. This suggests that lateral correlation among 1-D chains is remarkably developed and results in a three-dimensionally ordered array of 1-D chains. The diffuse scattering does not perfectly disappear even at 90 K. This may be attributed to the fact that interchain interactions are not strong enough to achieve long-range ordering. Cell dimensions including the superlattice reflections observed at 108 K can be estimated as triclinic, $a_{super} = 0.5a + 0.5b = 9.689$ Å, $b_{super} = -0.5a + 1.5b = 15.539$ Å, $c_{super} = 0.5a - 0.5b + c = 15.771$ Å, $\alpha_{super} = 98.965°$, $\beta_{super} = 103.474°$, $\gamma_{super} = 97.664°$, and $V_{super} = V = 2244.95$ Å^3.

Polarized Raman Spectra. The polarized Raman spectra of a single crystal of **3** at room temperature are shown in Figure 15 together with those observed for crystals of **1** and **2**. Attempts to calculate the vibrational frequencies of **3** using a cluster model based on DFT were unsuccessful. Therefore, geometry optimizations and vibrational frequency calculations for **1** and **2** were carried out based on DFT at the B3LYP level employing the LANL2DZ basis set, which is capable of performing calculations on third-row transition-metal complexes.[38] DFT calculations are also known to be successful in reproducing fundamental frequencies for large transition-metal compounds containing metal−metal bonds.[39] The calculated vibrational frequencies for **1** and **2** are listed in Supporting Information together with observed values from Raman spectroscopic measurements.

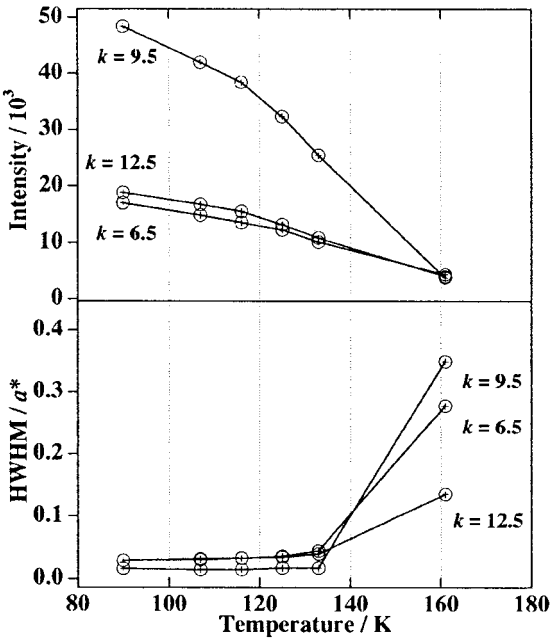

Figure 14. (a) Temperature dependence of the peak intensity of the $k = 6.5$, 9.5, and 12.5 scattering of **3**. (b) Temperature dependence of the half width at half-maximum (hwhm) along a^* of the $k = 6.5$, 9.5, and 12.5 scattering of **3**.

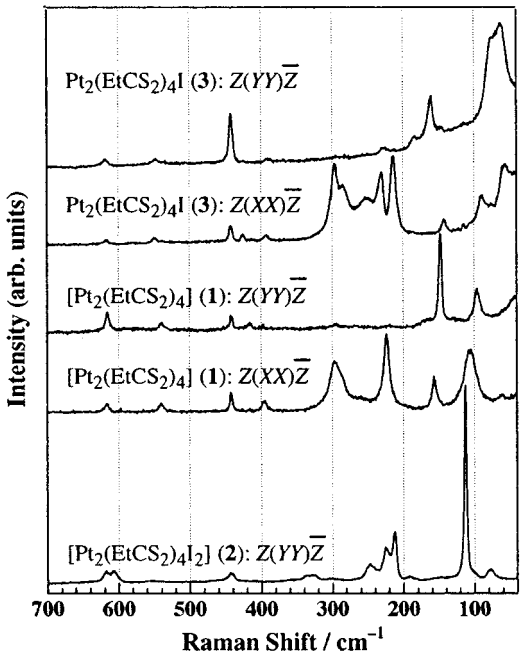

Figure 15. Polarized Raman spectra for the crystals of **1**, **2**, and **3** by 514.5-nm excitation at room temperature.

(32) (a) Comès, R. In *Chemistry and Physics of One-Dimensional Metals*; Keller, H. J., Ed.; NATO ASI Series, Series B.; Plenum Press: New York, 1977; Vol. 25, pp 315−339. (b) Pouget, J. P.; Comès, R.; Bechgaard, K. In *The Physics and Chemistry of Low Dimensional Solids*; Alcácer, L. Ed.; NATO ASI Series, Series C; D. Reidel Publishing: Dordrecht, The Netherlands, 1980; pp 113−121. (c) Pouget, J. P. In *Low-Dimensional Conductors and Superconductors*; Jérome, D., Caron, L. G., Eds.; NATO ASI Series, Series B; Plenum Press: New York, 1987; Vol. 155, pp 17−45. (d) Filhol, A. In *Organic Conductors*; Farges, J.-P., Ed.; Marcel Dekker: New York, 1994; pp 147−228. (e)Henriques, R. T.; Alcácer, L.; Pouget, J. P.; Jérome, D. *J. Phys. C: Solid State Phys.* **1984**, *17*, 5197−5208.

(33) (a) Comès, R.; Lambert, M.; Zeller, H. R.*Phys. Status Solidi B* **1973**, *58*, 587−592. (b) Comès, R.; Lambert, M.; Launois, H.; Zeller, H. R. *Phys. Rev. B* **1973**, *8*, 571−575. (c) Pouget, J. P.; Khanna, S. K.; Denoyer, F.; Comès, R.; Garito, A. F.; Heeger, A. J. *Phys. Rev. Lett.* **1976**, *37*, 437−440. (d) Khanna, S. K.; Pouget, J. P.; Comès, R.; Garito, A. F.; Heeger, A. J. *Phys. Rev. B* **1977**, *16*, 1468−1479. (e) Kagoshima, S.; Ishiguro, T.; Anzai, H. *J. Phys. Soc. Jpn.* **1976**, *41*, 2061−2071.

(34) Miller, J. S.; Epstein, A. J. *Prog. Inorg. Chem.* **1976**, *20*, 1−151.

(35) Kagoshima, S.; Nagasawa, H.; Sambongi, T. *One-Dimensional Conductors*; Springer Series in Solid-State Sciences; Springer-Verlag: Berlin, 1988; Vol. 72, Chapter 5.

(36) Sawatzky, G. A.; Antonides, E. *J. Phys. Colloq.* **1976**, *37*, C4, 117−123.

(37) (a) Nagasawa, H. *J. Phys. Soc. Jpn.* **1978**, *45*, 701−702. (b) Nagasawa, H. *Phys. Status Solidi B* **1982**, 109, 749−759.

(38) (a) Cui, Q.; Musaev, D. G.; Morokuma, K. *Organometallics* **1997**, *16*, 1355−1364. (b) Hill, G. S.; Puddephatt, R. J. *Organometallics* **1998**, *17*, 1478−1486. (c) Naka, A.; Yoshizawa, K.; Kang, S.; Yamabe, T.; Ishikawa, M. *Organometallics* **1998**, *17*, 5830−5835. (d) Su, M.-D.; Chu, S.-Y. *Chem. Phys. Lett.* **1998**, *282*, 25−28.

Table 6. Assignments of Bands Observed in the Polarized Raman Spectra of $Pt_2(EtCS_2)_4I$ (**3**)

Raman		
$Z(YY)\bar{Z}$	$Z(XX)\bar{Z}$	assignment
	57 (m)	Pt−Pt torsion
63 (s)		Pt−Pt−I bending
74 (s)		Pt−Pt stretching
	89 (m)	
114 (vw)		
	142 (m)	in-plane S−Pt−S bending
147 (w)		out-of-plane S−Pt−S bending
160 (s)		Pt−I stretching
184 (w)		
	213 (s)	Pt−S stretching
227 (w)	230 (m)	Pt−S stretching
	251 (m)	Pt−S−C bending
	284 (m), 296 (s)	Pt−S stretching
390 (vw)	392 (w)	Pt−S−C bending
442 (s)	442 (m)	in-plane S−C−S bending
547 (w)	548 (w)	out-of-plane S−C−S bending
618 (w)	617 (w)	out-of-plane S−C−S bending

According to DFT calculations, the two bands at 96 and 148 cm^{-1} observed in the Raman spectrum of **1** in the $Z(YY)\bar{Z}$ orientation are assigned to out-of-plane S−Pt−S bending and Pt−Pt stretching modes, respectively. Two relatively intense bands observed at 224 and 297 cm^{-1} in the $Z(XX)\bar{Z}$ orientation are assigned to ν(Pt−S) modes. The three bands at 442, 540, and 616 cm^{-1} are observed in both orientations. The first band is assigned to in-plane S−C−S bending and the last two bands to out-of-plane S−C−S bending modes. The Pt−Pt and Pt−I stretching modes of **2** are calculated at 102 and 193 cm^{-1}, respectively. An intense band at 112 cm^{-1} with overtones and a weak band at 192 cm^{-1} are assigned to the Pt−Pt and Pt−I stretching mode, respectively.

Assignments of the Raman bands of **3** were made using both the temperature dependence on the Raman spectra of **3** and calculations of **1** and **2** and are summarized in Table 6. The Raman spectra of **3** measured in the temperature range of 1.5−400 K in the $Z(YY)\bar{Z}$ orientation (1-D chain direction) are shown in Figure 16. A relatively intense band at 160 cm^{-1} exhibits a sudden and remarkable shift to higher wavenumber around 200 K (164 cm^{-1} at 200 K is shifted to 173 cm^{-1} at 175 K). As described previously, the lattice parameter *b* along the chain direction shows a sharp change around the transition temperature which corresponds to elongation of not the Pt−Pt but the Pt−I bond. Taking into account these experimental results, it is reasonable to assign the band at 160 cm^{-1} to the Pt−I stretching mode. Kitagawa et al. reported polarized Raman spectra of $Pt_2(dta)_4I$ and assigned an intense band at 68 cm^{-1} and a very weak band at 115 cm^{-1} to ν(Pt−Pt) and ν(Pt−I), respectively, while assigning the relatively intense band at 164 cm^{-1} to the δ(S−Pt−S) mode. A very weak band is also observed at 114 cm^{-1} for **3**, but the energy of this band shows little temperature dependence. The Raman spectra of **3** in the $Z(YY)\bar{Z}$ orientation shows two intense bands at 63 and 74 cm^{-1}. We assign the former band to the Pt−Pt−I bending mode and the latter to the Pt−Pt stretching mode. It should be noted that Raman spectra above 200 K exhibit broadening of the bands. This may be a result of the fact that vibronic interaction plays an important role in the metallic state.

Magnetic Properties. The temperature dependence of the magnetic susceptibility of **3** is shown in Figure 17. The

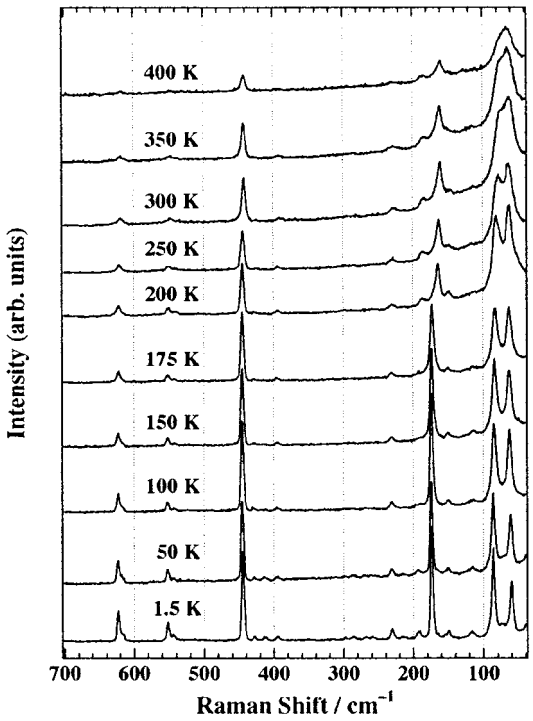

Figure 16. Temperature dependence of the polarized Raman spectra of a single crystal of **3** in $Z(YY)\bar{Z}$ orientation obtained by 514.5-nm excitation.

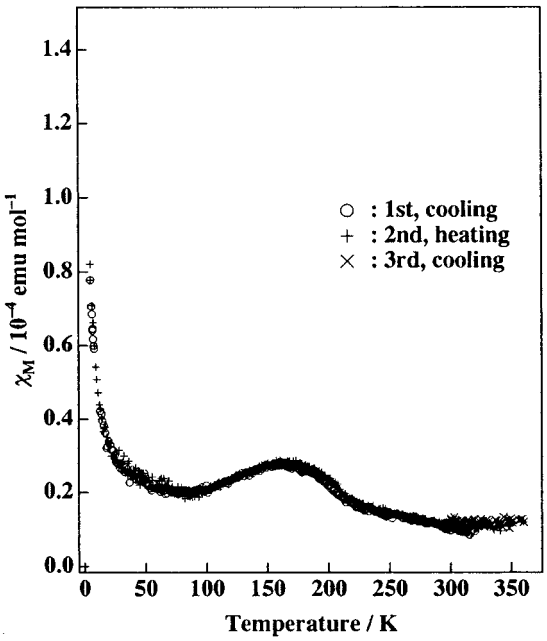

Figure 17. Temperature dependence of the magnetic susceptibility of **3**.

reproducibility of the magnetic data was confirmed. Magnetic susceptibility in the semiconducting state below 205 K is of the order of $\sim 2 \times 10^{-5}$ emu mol^{-1}.[40] As previously described, this compound shows diffuse scattering corresponding to valence-ordering of $-Pt^{2+}-Pt^{2+}-I-Pt^{3+}-Pt^{3+}-I-$ or $-Pt^{2+}-Pt^{3+}-I-Pt^{3+}-Pt^{2+}-I-$ and this diffuse scattering is transformed to superlattice reflections below T_{M-S}. The former valence-ordering mode is formally the diamagnetism because

(39) (a) Cotton, F. A.; Feng, X. *J. Am. Chem. Soc.* **1998**, *120*, 3387−3397. (b) Cotton, F. A.; Feng, X. *J. Am. Chem. Soc.* **1997**, *119*, 7514−7520.

(40) Magnetic susceptibility of **3** at room temperature is $\sim 1.1 \times 10^{-5}$ emu mol^{-1}, which is nearly in accordance with the value determined by the EPR measurement ($\sim 1.3 \times 10^{-5}$ emu mol^{-1}). Tanaka, H.; Marumoto, K. Kuroda, S.; Mitsumi, M.; Toriumi, K., manuscript to be submitted.

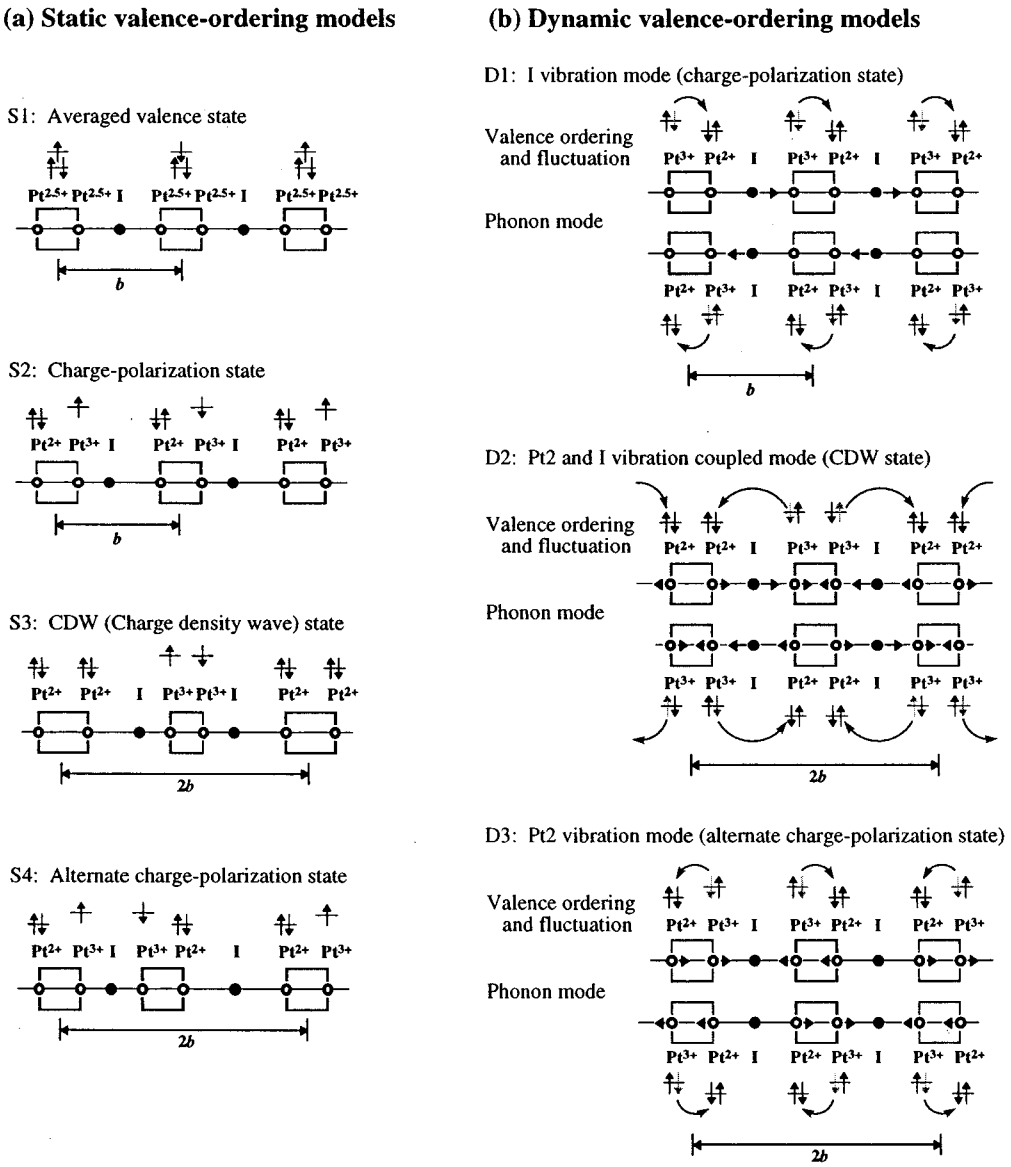

Figure 18. Static valence-ordering models (a) and dynamic valence-ordering models (b) proposed for **3**.

of the $d\sigma^2 d\sigma^{*0}$ configuration of the tervalent diplatinum unit. However, it would not become perfectly diamagnetic if the valence states of the platinum atoms were close to +2.5 by the interaction between diplatinum units through the bridging iodine atom. In the latter case, it is considered that spins of the tervalent platinum ions strongly interact antiferromagnetically by the overlap of orbitals through the iodine atoms. Therefore, the very small value for magnetic susceptibility in the semiconducting region can be interpreted as resulting from spins that are nearly canceled by adopting 2-fold periodical ordering. Magnetic susceptibility exhibits changes in slope near the transition temperature and a slight swelling near 160 K. As described in the X-ray Diffuse Scattering section, lateral correlation among 1-D chains rapidly develops in this temperature region. The swelling observed in magnetic susceptibility seems to have appeared concerning the rapid development of the lateral correlation, though a clear explanation is not possible at this time. The spin degree of freedom survives at low temperature, and loss of the spin degree of freedom accompanied by the transition to the ground state of $-Pt^{2+}-Pt^{2+}-I-Pt^{3+}-Pt^{3+}-I-$ or $-Pt^{2+}-Pt^{3+}-I-Pt^{3+}-Pt^{2+}-I-$ has not been observed. The lack of evidence for such a ground state down to 2 K for the present compound should be interpreted as a large fluctuation effect due to high one-dimensionality. The tail, observed in the χ_M versus T plot below ~25 K may arise from paramagnetic centers originating from impurities or lattice defects. Kitagawa et al. assigned the origin of the metal−semiconductor transition observed for $Pt_2(dta)_4I$ to a Mott−Hubbard transition ($4k_F$-CDW) from the temperature dependence of magnetic susceptibility.[10c,d] However, it is considered that the solid-state properties of our compound cannot be perfectly understood by a simple 1-D band model.

Valence-Ordering Models. Generally, 1-D conductors form uniform structures in the metallic state but change upon metal−semiconductor transitions such as the Peierls transition to structures with lattice distortion. However, it has been revealed from crystal structure analyses and diffuse scattering measurements that **3** has a lattice distortion owing to the dynamic or static distortion of the bridging iodine atom above the transition temperature. This is completely opposite to the usual behavior of 1-D conductors. A possible valence-ordering model in the metallic state can be proposed based on the experimental results described above, though decisive evidence has not yet been obtained. As previously described in the Introduction, the possible electronic structures of MMX chain compounds can be represented by the four static valence-ordering models S1−

S4 shown in Figure 18. Models S3 and S4 accurately reproduce the periodic ordering with 2-fold repetition length of the MMX unit, which was revealed by diffuse scattering with $k = n + 0.5$ (n; integer). On the other hand, crystal structure analyses of **3** have revealed that all the Pt−Pt distances are crystallographically identical, that the two Pt−I distances are equivalent within experimental errors, and that U_{22} of the iodine atom becomes exceptionally large above T_{M-S}. The S3 model explains the crystal structure if positional disorder of the bridging iodine atom is brought about through weak interchain interactions similar to those in $Pt^{II}-Pt^{IV}$ mixed-valence compounds. However, the perfectly filled band would not lead to metallic behavior. In S4, positional disorder of the platinum atom instead of the bridging iodine atom must be expected if structural misalignment among linear chains is concerned in the crystal structure. The exceptionally large temperature factor U_{22} of the iodine atom along the linear chain direction can also be interpreted by the dynamic valence-ordering models, rather than the static ones, shown in Figure 18, in which the valence fluctuation and phonon vibration are coupled with each other. It is well known that the $Pt^{3+}-Pt^{3+}$ diplatinum complex has two halogen ions at apical positions but the apical positions of the $Pt^{2+}-Pt^{2+}$ complex are vacant. If the bridging iodine atom of the MMX chain compound were shifted from being bound to Pt^{3+} to a position close to the neighboring Pt^{2+}, electron transfer from Pt^{2+} to Pt^{3+} would be induced. This electron transfer is a result of the strong coupling between the coordination geometries of the Pt complexes and their valence states, so-called electron−phonon coupling. The D1 model is the iodine vibration mode but does not correspond to 2-fold periodical ordering. The D3 model is the vibration mode of the diplatinum unit, whereas D2 is the mode in which the stretching of Pt−Pt bonds and the shifts of the bridging iodine atoms positions are strongly coupled. Although the D3 model can reproduce the 2-fold periodical ordering, the large U_{22} of Pt rather than that of I must be expected. From the viewpoint of 2-fold periodical ordering and the large U_{22} of the iodine atom, model D2 appears to be the most appropriate model in representing the valence-ordering state of **3**. The dynamic valence-ordering state proposed here should be a very attractive one, but further detailed experimental and theoretical studies may be required.

Kitagawa et al. have assigned the valence-ordering state of $Pt_2(dta)_4I$ on the basis of polarized Raman, IR spectroscopy, and magnetic susceptibility measurements.[10c,d] The valence-ordering modes of $Pt_2(dta)_4I$ were considered to be $-Pt^{2.5+}-Pt^{2.5+}-I-Pt^{2.5+}-Pt^{2.5+}-I-$ for the metallic phase above T_{M-S} and $-Pt^{2+}-Pt^{3+}-I-Pt^{2+}-Pt^{3+}-I-$ for the semiconducting phase below T_{M-S}. The interpretation of the valence-ordering mode for the metallic state in **3** is different from that in $Pt_2(dta)_4I$ but appears to be due to differences between the time scales of measurements. The time scale of Raman and IR spectroscopy is in the order of 10^{-13} s, while X-rays with wavelengths of 0.5 Å interact with the atom in 2.3×10^{-16} s. Actually, diffuse scattering corresponding to periodic ordering with 2-fold repetition length of the MMX units has also been observed in $Pt_2(dta)_4I$.[11] On the other hand, valence ordering in the low-temperature insulating phase below 80 K of $Pt_2(dta)_4I$ was assigned to $-Pt^{2+}-Pt^{3+}-I-Pt^{3+}-Pt^{2+}-I-$ on the basis of ^{129}I Mössbauer spectroscopy. Recently, we have succeeded in the synthesis of the new MMX compound, $Pt_2(n\text{-}BuCS_2)_4I$, which shows first-order phase transitions near 209 and 321 K.[41] Low-temperature crystal structure analysis below 209 K has revealed a 1-D chain composed of 2-fold periodical ordering of the MMX units represented by $-Pt^{2+}-Pt^{3+}-I-Pt^{3+}-Pt^{2+}-I-$. Furthermore, theoretical studies on the valence state and structural distortions in MMX compounds have been described.[42,43] Borshch et al. have reported that, based on the phenomenological chain and cluster models, the valence distortion of $Pt_2(dta)_4I$ is $-Pt^{2+}-Pt^{3+}-I-Pt^{3+}-Pt^{2+}-I-$.[43a] Considering these results, the most probable ground state of **3** may be the valence state of $-Pt^{2+}-Pt^{3+}-I-Pt^{3+}-Pt^{2+}-I-$.

Conclusions

We have reported the synthesis, crystal structure, solid-state behavior, and a number of novel properties of the infinite linear chain halogen-bridged mixed-valence diplatinum complex, $Pt_2(EtCS_2)_4I$ (**3**), such as metallic conducting behavior and periodic valence ordering. In accordance with the metal−semiconductor transition, remarkable anomalies in the temperature dependence of the crystal structures, lattice parameters, X-ray diffuse scattering, polarized Raman spectra, and magnetic susceptibility are observed near T_{M-S}. X-ray crystallographic studies of **3** as a function of temperature revealed the presence of a lattice distortion owing to periodic valence ordering along the 1-D chain even in the metallic regime, while dimensionality of the valence ordering changed along with the metal−semiconductor transition. To correlate physical properties to the crystal structure of the unusual compound **3**, valence-ordering models have been examined and the dynamic valence-ordering model D2 is proposed. However, further detailed studies are required to obtain unambiguous evidence. Further studies with the MMX chain compounds, $Pt_2(RCS_2)_4I$, in which methyl groups of dithioacetate ligand are replaced by another alkyl or phenyl group, are ongoing.

Acknowledgment. This work was supported by a Grants-in-Aid for Scientific Research from the Hyogo Prefecture and Grants-in-Aids for Scientific Research (10740307 and 09440232) and on a Priority Areas "Metal-Assembled Complexes" (11136244) from the Ministry of Education, Science, Sports and Culture, Japan. We thank Professor Hisayoshi Kobayashi at Kurashiki University of Science and the Arts for his useful advice concerning Gaussian98 calculations.

Supporting Information Available: CIF for all data sets, packing diagrams for **2** and **3**, and calculated and observed vibrational frequencies for **1** and **2** (PDF). This material is available free of charge via the Internet at http://pubs.acs.org. See any current masthead page for ordering information and Web access instructions.

JA010900V

(41) Mitsumi, M.; Kitamura, K.; Morinaga, A.; Ozawa, Y.; Kobayashi, M.; Toriumi, K.; Iso, Y.; Kitagawa, H.; Mitani, T., manuscript to be submitted.

(42) Whangbo, M.-H.; Canadell, E. *Inorg. Chem.* **1986**, *25*, 1726−1728.

(43) (a) Borshch, S. A.; Prassides, K.; Robert, V.; Solonenko, A. O. *J. Chem. Phys.* **1998**, *109*, 4562−4568. (b) Robert, V.; Petit, S.; Borshch, S. A. *Inorg. Chem.* **1999**, *38*, 1573−1578. (c) Kuwabara, M.; Yonemitsu, K. *Physica B* **2000**, *284*−*288*, 1545−1546. (d) Kuwabara, M.; Yonemitsu, K. *J. Phys. Chem. Solids* **2001**, *62*, 435−438.